

Numerical modelling of Venus' mantle: the role of cratons in lithospheric overturns

Rebecca Vilde Martine Krohn Karlsson



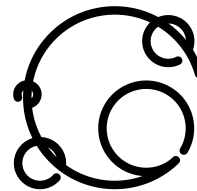
Master's thesis in Geoscience
Geophysics Program
60 credits

Department of Geosciences
Faculty of Mathematics and Natural Science
UNIVERSITY OF OSLO
Norway
Spring 2019

Numerical modelling of Venus' mantle: the role of cratons in lithospheric overturns

by

Rebecca Vilde Martine Krohn Karlsson



©2019 Rebecca Vilde Martine Krohn Karlsson

Numerical modelling of Venus' mantle: the role of cratons in lithospheric overturns

Supervisors: Prof. Stephanie Werner and PhD candidate Sruthi Uppalapati

<http://www.duo.no/>

Printed: Reprosentralen, University of Oslo

Abstract

Despite its similarities in bulk properties to Earth, Venus portrays a fundamentally different mode of surface tectonics. Venus is currently known to be operating in stagnant lid mode of mantle convection. However, it is debated to have an episodic lid regime with long quiescent periods, broken by rapid subduction-driven plate recycling, that recycles the crust globally over geologically short periods of time. However, the tesserae regions, that cover approximately 10 % of the surface of the planet may be older than the remaining surface. The composition and age of the tesserae are still unknown, but they are observed to be strongly deformed and might therefore have survived the global recycling events. It has therefore been suggested that these tesserae may in some ways be comparable to continents on Earth, since these are areas that do not participate in subduction.

Based on previous work on mantle convection modelling on Venus with and without cratons, this project aims to further the knowledge of possible cratons on Venus and their impact on the mantle dynamics and proposed overturn events. By thermochemical modelling carried out with the StagYY code, models with a varying number of cratons and varying yield stress are produced in 2D and 3D. The cratons' impact on the mantle is investigated by examining the number of mantle plumes, the thermal evolution, the crustal thickness and the surface age. The findings show that the number, timing and mode of overturns are highly dependent on yield stress and in some degree dependent on pre-imposed cratons. The cratons have a significant effect on the wavelength of convection in the mantle, which may lead to changes in plume patterns and overturn initiation.

Acknowledgements

I would like to thank my supervisors, Stephanie Werner and Sruthi Uppalapati for taking me on as a master student and letting me work on such an interesting and fun project. Special thanks to Fabio Cramer and Tobias Rolf for contributing with their expertise and valuable input. I would also like to thank my fellow master students and Space Girls, Kristina and Michael. Kristina, for bringing the coffee machine and making me aware of all the birds in the tree outside the office, and Michael for providing bad jokes, keeping our spirits up. Lastly, thanks to my boyfriend, Helge, and the rest of my family for amazing motivation and support.

Contents

1	Introduction	1
1.1	Venus geology	2
1.2	Tesserae	5
1.3	Tesserae age	6
1.4	Tesserae formation	7
1.5	Geodynamic modelling	8
1.6	Objectives and motivation	10
2	Method	11
2.1	Numerical model	11
2.2	Model setup	11
2.2.1	Boundary conditions	11
2.2.2	Rheology	12
2.2.3	Minerology	14
2.2.4	Partial melting	14
2.2.5	Pre-imposed cratons	15
2.3	Diagnostics	16
2.3.1	Visualisation	17
3	Results	18
3.1	Overturn episodes	19
3.2	Mode of overturns	27
3.3	Thermal evolution	31
3.4	Plumes	35
3.5	Crustal thickness	44
3.6	Surface age	50
3.7	3D models	56
4	Discussion	59
4.1	Stagnant and episodic lid	59
4.2	Mode of overturns	61
4.3	Thermal evolution	62

4.4	Plumes	62
4.5	Crustal thickness and surface age	63
4.6	3D models	65
4.7	Comparison to Venus	65
5	Conclusions	67

List of Figures

2	Venus stratigraphy (Ivanov and Head, 2011).	4
3	Tessera regions map (Ivanov and Head, 2011)	5
4	Initial temperature and viscosity	13
5	Initial distribution of cratons	18
6	Evolution of reference model	19
7	Comparison: number of slabs vs surface mobility	20
8	Detection of slabs	21
9	Number of plumes	26
10	Overturn, no cratons and 80 MPa yield stress	28
11	Overturn, one craton and 80 MPa yield stress	29
12	Horizontal velocity, one craton, 80 MPa yield stress	30
13	Overturn, two cratons and 80 MPa yield stress	30
14	Overturn, three cratons and 40 MPa yield stress	31
15	Mean mantle temperature, same yield stress	33
16	Mean mantle temperature, same number of cratons	35
17	Plume detection	36
18	Number of plumes at mid-mantle depth.	40
19	Plume detection, one craton and infinite yield stress	41
20	Horizontal velocity for infinite yield stress cases	42
21	Viscosity, horizontal and radial velocity, zero and one craton.	43
22	Crustal thickness, infinite yield stress and different number of cratons	44
23	Crustal thickness at 2.45 and 2.60 Gyr, one craton and 150 MPa yield stress	45
24	The spreading ridge, close to the craton.	46
25	Mean crustal thickness, infinite yield stress and different number of cratons	47
26	Crustal thickness for areas without cratons.	49
27	Surface ages trough time	53
28	Surface distribution at 1 Gyr	54
29	Surface distribution during overturn.	55
30	Viscosity of the evolution in the same case as figure 29.	56
31	3D evolution of overturn	57
32	Subducting slab during the overturn event in Figure 31.	58

List of Tables

1	Model parameters	14
2	Overview of models with overturns	20

1 Introduction

Venus is similar to Earth in size, bulk composition and distance from the Sun, however there are some distinct differences, both on the surface and in the interior. The planet has a high surface temperature of 450°C and a dense atmosphere. The atmosphere is about 90 times as thick as that of Earth, and is largely composed of CO_2 (96%) and N_2 (3.5%), causing a runaway greenhouse effect. The thick clouds of Venus consists of 75% sulphuric acid and 25% water vapour (Donahue and Russell, 1997). Venus' atmosphere in total only contains 1-100 ppm water, but the hydrogen-deuterium ratio supports theories that the planet might have had an ocean, long since evaporated, causing H_2 to escape into space (Nimmo and McKenzie, 1998). Venus currently operates in stagnant lid mode, meaning that the planet is covered by one connected, rigid plate. There are however some signs of convergent plate boundaries (Cramer, 2017) in the form of trenches at the edges of corona structures (Davaile et al., 2017). It is clear that these observations suggest a different evolution from Earth, which is in mobile lid mode. Here plate tectonics, with multiple plates, subduction and mid-oceanic spreading, is presently active. However, the stagnant lid of Venus is proposed to be broken up by periods of rapid subduction, creating a transitional regime, an episodic lid that functions in between a mobile and a stagnant lid (Turcotte, 1995).

Venus' thick cloud cover makes observation from space difficult. However, through the 70's and early 80's the Venera and Vega missions gathered the first bits of information on the atmosphere and surface (Basilevsky et al., 2007). This was continued with the Magellan mission that gave the first high resolution radar images from space, covering 97% of the surface, in addition to providing gravity and altimetry data. More recently, Venus Express was launched to provide more in-depth data on Venus' atmosphere (Svedhem et al., 2007). Instruments focused on thermal measurements, both in the atmosphere and on the surface were included to examine Venus' recent resurfacing history among other things (Smrekar et al., 2010). All of these collected data give the foundation for understanding volcanism, tectonism, impact processes and surface processes on the planet.

Tectonic surface expressions on Earth, like mid oceanic ridges, subduction zones, mountain chains and large lava flows, are often obscured by vegetation or eroded by wind and

water, in addition, large parts of the surface is rejuvenated continuously. This makes old tectonic and volcanic features on Earth difficult to study. On Venus however, these structures are less obscured, due to differences in atmospheric conditions. The high temperatures makes retention of water on the surface impossible. The winds close to the surface of Venus have a velocity of only ~ 1 m/s, suggesting that the surface erosion is limited (De Pater and Lissauer, 2015). As on Earth, the number of impact structures on the surface is low, and they generally do not obscure the tectonic and volcanic structures on the surface (Ivanov and Head, 2013). These conditions make Venus the perfect place to study tectonic and volcanic structures without the interference of other elements. These studies can unlock Venus' thermal evolution and geological history and give important insight into the early evolution of terrestrial planets.

1.1 Venus geology

Mapping the geology of Venus following the dual stratigraphic classification approach (Ivanov and Head, 2011), gives the foundation for studying the planet's volcanic and tectonic history. Different units were observed from the Magellan SAR images, and built up into a global stratigraphic column (Figure 2). Venus' geological history can be separated into three major phases. The Fortunian phase is dominated by intense deformation and the formation of tesserae. Tesserae regions cover approximately 10 % of the surface and are situated above the mean planetary radius (MPR). The second phase, the Guineverian, is distinguished by the emplacement of vast regional plains that cover approximately 70 % of the surface. Based on observations of their morphology the volcanic plains are likely to have a basaltic composition (Nimmo and McKenzie, 1998). Between the plains are large ridge belts, which can be thousands of km long and are signs of folding and shortening. Wrinkle ridges were also formed during this period, probably caused by compression (Basilevsky and Head, 2003). The third phase, the Atlian, is associated with the formation of rift zones and large shield volcanoes. This time period shows a decrease in volcanism compared to the Guineverian, and this volcanism may have been active up to recent geologic time. These different phases are recognisable globally and the stratigraphic column mostly follows the same pattern throughout planet (Ivanov and Head, 2011).

An important part of the study of terrestrial planets is to understand how they lose internal heat. Earth loses heat mostly through plate tectonics, i.e. the subduction of cool oceanic lithosphere. Other terrestrial planets, like Mars, loses their heat through conduction and possibly magmatism. This is because the lithosphere consists of a single thick plate that does not break up or subduct. The heat loss mechanism on Venus can have several explanations. The first possibility is that Venus loses its heat in a steady state mechanism, where the heat is exchanged from the mantle to the surface, through convection, conduction and volcanism. However, this mechanism demands a very high plume flux or rapid delamination of the lithosphere and is therefore seen as highly unlikely. The second possible method is a concentration of heat producing elements in the upper crust, and heat only loss by conduction, which is also not considered likely. The third mechanism is heat loss by rapid periods of subduction. These are then interrupted by long quiescent periods where the planet is in stagnant lid mode, which is known as episodic lid mode. This theory is supported by the surface age of 500 ± 200 Myr assumed by the near random crater distribution (Strom et al., 1994; Schaber et al., 1992). The equal distribution of impact craters on Venus suggests that the whole surface must have been renewed in a short period of time. Equilibrium resurfacing through volcanism, would renew different areas of the surface at different times. The distribution of craters would then not be random, in contrast to their predicted distribution for the global resurfacing method (Romeo and Turcotte, 2010).

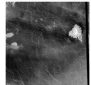
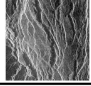

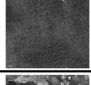
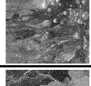
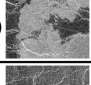
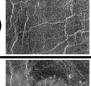
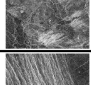
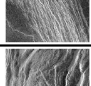
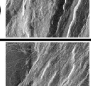
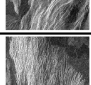
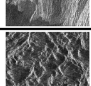

Geologic time units	Time-stratigraphic units	Rock-Stratigraphic units and structures
Atlian Period	Atlian System	Aurelia Formation (dark parabola) 
		Devana Formation (rz) 
		Atla Group
		Bell Formation (pl) 
		Gunda Formation (ps) 
		Boala Formation (sc) 
Guineverian Period	Guineverian System	Rusalka Group
		Ituana Formation (rp2) 
		Rusalka Formation (rp1) 
		Accruva Formation (psh) 
		Agrona Formation (gb) 
		Lavinia Group
		Akna Formation (mb) 
		Lavinia Formation (pr) 
		Atropos Formation (pdl) 
Fortunian Period	Fortunian System	Fortuna Formation (t) 
Pre-Fortunian Period	Pre-Fortunian System	?

Figure 2: Venus stratigraphy, showing the geological time scale of Venus. T signifies the mean model absolute age of the surface. This value is not specified due to the difficulties of exactly dating Venus' surface (Ivanov and Head, 2011).

1.2 Tesserae

Tesserae regions cover approximately 10 % of the surface of Venus. They are defined by their high degree of deformation which is interpreted to be caused by initial shortening followed by extension (Brown and Grimm, 1997), including at least two intersecting sets of structures, graben and fractures (extensional) and ridges (contractual). The surface is rough and has a high radar back scatter. Tesserae are mostly located in certain areas on the surface, in and around Ishtar Terra, the Alpha-Thetis region and the Nemesis-Phoebe region (Figure 3). As these structures are partly covered by volcanic plains, they are proposed to be some of the oldest structures on the surface. Because of their high elevation the volcanic plains do not cover them completely, but embay them (Ivanov and Head, 2011). It is suggested that the tesserae regions may be compared to Archean continents on Earth. Earth and Venus may have began their evolution in a similar way, with production of cratons by major plume activity or other formation mechanisms (Harris and Bédard, 2014; Romeo and Turcotte, 2008). Earth then developed plate tectonics, while Venus probably developed an episodic lid. Venus may therefore be comparable to pre-plate tectonic Earth (Hansen, 2015). However, too little is known about tesserae to state this with any certainty.

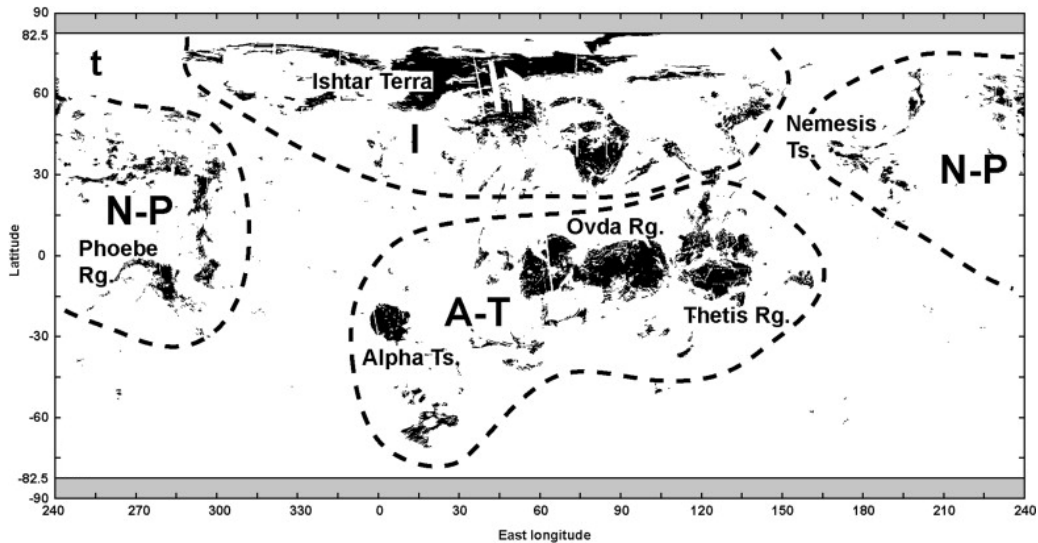


Figure 3: Tesserae regions; dotted lines show clusters: I - Ishtar cluster, A-T - Alpha-Thetis cluster, N-P - Nemesis-Phoebe cluster (Ivanov and Head, 2011)

1.3 Tesserae age

It is difficult to determine the exact age of Venus' surface with the data available today. The relative ages of tesserae regions may, however, be inferred from the stratigraphy and the cratering record. The stratigraphic interpretation shows the tesserae as the oldest structures, being overlapped by volcanic plains (Brown and Grimm, 1997). The cratering record may give some indication of the total age of the surface of Venus, however, only if certain other assumptions are taken into account (Campbell, 1999). The difference in crater density on separate geological structures may help estimate the difference in surface ages between them (Ivanov and Head, 2011). Venus' dense atmosphere prevents most small impactors reaching the surface, mainly creating craters > 32 km in diameter. However, owing to the low erosion rate on Venus, the existing craters are usually well preserved, only being damaged by tectonic processes and volcanism (Bindschadler, 1995). Even though the cratering densities on Venus are near indistinguishable from a random distribution, a look at the density differences of separate geological areas show some variation in age (Kreslavsky et al., 2015). There are 1.4 times as many craters >16 km on the tesserae than elsewhere on Venus, supporting an older surface age for the tesserae. For small craters (<16 km) the density is lower on the tesserae than on the remainder of the planet. This is likely due to the difficulty of recognising craters on the rough surface of tesserae and is therefore a possible observational bias (Ivanov and Basilevsky, 1993).

Romeo and Turcotte (2008), on the other hand, point out that the amount of craters is too similar to expect a significant difference in formation age of the plains and the tesserae. Formation of tesserae and volcanic plains may therefore be linked. The reason for lack of craters on the tesserae is that they suffered great deformation in the form of shortening, shortly after a global overturn event. This may have erased all pre-existing craters on the surface, resetting the cratering record. Later impacts then produced craters on the newly formed volcanic plains and the tesserae at the same rate. The question still remains whether the tesserae are substantially older than the volcanic plains surrounding them.

1.4 Tesserae formation

Continents on Earth consists of granitic material, they are buoyant and lighter than the basaltic, oceanic crust. Through plate tectonics, the oceanic plate subducts underneath the continental plate, which remains on the surface. The crustal plateaus on Venus, where the tesserae are situated, may resemble these continental plates on Earth. They are different than the surrounding areas in both altitude and surface radiance, supporting a more felsic composition (Gilmore et al., 2017). However, it is not known whether the tesserae are in fact granitic. If the tesserae are comparable to Earth's cratons, then their formation might also be similar. The formation of the Archean cratons is still debated, cratons may have formed by the melting of hot ambient mantle (Herzberg and Rudnick, 2012), or by major plume activity (Campbell and Griffiths, 2014; Harris and Bédard, 2014).

Romeo and Turcotte (2008) propose that the cratons on Venus were formed in a thin lithosphere, early in the evolution of the planet, and are therefore older than the remaining surface. They also propose that they are pulsating continents, not recycled during overturn events, but growing and diminishing in cycles depending on the thickness ratio between crust and lithospheric mantle. If the crustal thickness is less than $2/5$ of the lithosphere thickness, the area will be compressed, but if it is larger, the area will be spread out and collapse. Because of these different events the plateaus and tesserae inliers can be interpreted to be the same structure, in different stages of the cycle. Inliers are made during spreading and collapse, when the lithospheric mantle under the craton is delaminated. Depending on the thickness ratio, this can happen during global overturn events. Plateaus are made if the lithospheric mantle remains and there is no delamination, causing compression and shortening.

Hansen (2018) suggests that there are several points about craton formation that the pulsating continent model does not address, and instead proposes another formation model. They show that plateaus on Venus and Archean cratons on Earth may have formed by a bolide impact. This impact into the lithosphere, which was thinner than it is today, may have penetrated right down to the mantle and caused extensive melting, creating enormous lava ponds. The plateaus then formed when the slag at the surface of

the lava ponds started cooling and produced deformations in different wavelengths. For the cooling lakes to become plateaus, they had to remain coupled to their root, otherwise they would subside to the mean planetary elevation (Hansen, 2015). The details on tesserae formation still remains unclear.

1.5 Geodynamic modelling

The similarity in size to Earth makes it possible for Venus to sustain long-lasting volcanism, unlike smaller terrestrial bodies, like Mars and Moon. Venus also has clear signs of tectonic processes, like trenches that resembles Earth's subduction zones (Fowler and O'Brien, 2003; Cramer, 2017). Even though their tectonic mode is vastly different, the comparison between Venus and Earth can help constrain the geological evolution of both Earth and other terrestrial planets (Ivanov and Head, 2013). Earth has a mobile lid, whereas Venus is currently in stagnant lid mode. The stagnant lid mode of Venus is proposed to be broken up by episodes of rapid global or nearly global subduction, thereby having an episodic lid. Venus may therefore have a tectonic mode in between that of Earth (mobile lid) and the smaller terrestrial planets in our solar system (stagnant lid). There are several possible explanations for the differences in the tectonic mode of the two planets. Venus' higher surface temperature (Bercowski and Ricard, 2014), lower water content or simply bi-stable planetary evolution, where different tectonic modes are plausible are some of the suggestions (Weller et al., 2015).

Since there is no seismic data and only limited compositional information available for Venus, surface images, gravity and altimetry data are the most important sources of insight into the interior of the planet. Numerical modelling is a useful tool to understand how the evolution of the planet has led it to its current state. Models compared to observational data can give good constraints on the evolutionary history of Venus. Where information from the planetary interior needed for Venus modelling is unattainable, knowledge of Earth is utilised and adapted.

To test the theory of episodic lid convection for Venus, comparisons of crustal thicknesses attained from observational data and numerical models have been carried out. Estimates of the crustal thickness vary with the different assumptions of Venus interior.

The two original sources for estimates about the crustal thickness were the spacing of tectonic structures and the depth of impact craters. These methods yielded mean crustal thicknesses lower than 20 km (Phillips and Hansen, 1994). Based on spectral admittance modelling, the crustal thickness has been suggested to range from 0 - 90 km (Anderson and Smrekar, 2006). Estimating the crustal thickness inferred by geoid and topography yields mean crustal thickness results of 8 - 25 km (James et al., 2013), while Smrekar et al. (2010) assumes a higher value of mean crustal thickness of ~ 60 km.

The crustal thickness has also been modelled by several authors using both a stagnant lid approach and an episodic lid approach. Estimates based on stagnant lid modelling yielded values of 20 - 60 km (Orth and Solomatov, 2012), 40 - 100 km (Armann and Tackley, 2012) and > 100 km (Rolf et al., 2018). The episodic models yield generally lower values of crustal thickness 10 - 50 km (Armann and Tackley, 2012) and 40 - 60 km (Rolf et al., 2018). According to these results, the crustal thickness models based on episodic lid modelling closer resemble the estimated values from observational data and is therefore the most reasonable.

To further the understanding of the episodic lid mode of Venus, the planet's evolution has been modelled by several authors and compared to estimated surface age, topography and geoid. For the 2D episodic model of (Armann and Tackley, 2012) the best fit with estimates was a model with 5-8 overturns each lasting 150 Myr. Rolf et al. (2018) also carried out mantle modelling of Venus' interior. They looked into possible evolutionary paths that bring Venus to its present state, as far as this is known from observational data. Both stagnant and episodic lid models were examined. The results for the episodic lid model pointed towards an evolution with at least one overturn event ending a rather long time ago, maybe as much as 1 Gyr. The episodic models match the assumed crustal thickness ($\sim 40 - 60$ km) and the surface age (~ 500 Myr) better than the stagnant lid model. However, none of these above discussed approaches has considered tesserae regions and their possible survival through overturn periods.

As stated earlier, the tesserae regions may be the oldest remaining surfaces on Venus and may have survived at least the last overturn event. If they are in fact similar to

cratons, comparable to Earth’s continents, it is interesting to examine their role in the overturn events. Did they simply survive? Did their presence alter the mode or timing of the events or other aspects of the mantle dynamics? Cheng et al. (2018) have carried out numerical modelling of Venus with imposed cratons. These 2D models include one and two cratons that cover the surface with 10% total in both stagnant lid and episodic lid. The models were compared to reference models without cratons. Their goal was to examine whether the cratons could survive the overturn events and if they had any impact on them. They concluded that the imposed cratons may increase the surface velocity and cause an increase in global overturns. Numerical modelling with cratons is more extensively done for Earth. The work of Rolf et al. (2012) investigates super-continent cycles and makes it clear that the cratons have an impact on the mantle in the form of a heterogeneity that can change both temperature and flow patterns.

1.6 Objectives and motivation

This study continues the work on thermochemical evolution of Venus’ mantle with cratons. Varying the number of cratons and yield stress in 2D and 3D models and examining different aspect of the mantle evolution, will give insight into cratons’ impact on global overturn events and mantle dynamics.

Some of the questions that will be addressed here are:

- How do the pre-imposed cratons affect the mantle dynamics of Venus?
- Do pre-imposed cratons affect the timing and mode of episodic overturns?

2 Method

2.1 Numerical model

The StagYY code (Tackley, 2008) is used to carry out thermochemical convection modelling within planetary interiors. The code uses a staggered grid, where variables, such as temperature and pressure are defined at the centres of each grid cell and velocities are defined at the cell interfaces perpendicular to the respective velocity component. That means the radial velocities are offset by half a grid cell in the radial direction, while the respective horizontal velocities are offset by half a grid cell in the horizontal direction. Physical properties, like composition, are carried by tracers, the tracer density is converted to a continuous field. Numerical models can be carried out in both 2D and 3D geometry, using a spherical annulus geometry (Hernlund and Tackley, 2008) and a Yin Yang grid (Tackley, 2008) respectively. The governing equations; conservation of mass, momentum and energy are solved for the velocity components (two in 2D and three in 3D), pressure and temperature.

2.2 Model setup

Numerical models were carried out in both 2D and 3D, using a spherical annulus geometry (Hernlund and Tackley, 2008) and a Yin Yang grid (Tackley, 2008) respectively. The model setup is similar to that of Rolf et al. (2018), with some modifications. Most models are calculated in 2D to reduce computational time and additional models are calculated in 3D for comparison. The 2D resolution is set to 512×64 cells, whereas the 3D models have a lower resolution of $64 \times 192 \times 64 \times 2$ to reduce the computation time. The number of tracers, adjusted for the resolution, is set to 6438600 for the 2D cases and 1.44×10^8 for the 3D cases. Model parameters specific for Venus are shown in Table 1, additional parameters can be found in Rolf et al. (2018).

2.2.1 Boundary conditions

Free-slip boundary conditions are employed for both the top and bottom boundaries in all models. Some simplifications are made to the model concerning heating. The internal, radiogenic heating is constant and uniform throughout the mantle, whereas in a realistic planet it would decrease with time because of decay of heat producing materials and also

change with depth. The temperatures at the top and bottom boundaries are also constant, rather than changing with interactions with the core. Varying internal heating and bottom boundary temperature can be applied to make the models more realistic (Rolf et al., 2018), however, in this project the interest lies in the more general processes and this added realism is unnecessary.

The same initial conditions are used throughout all the modelled cases. The temperature increases from the surface, through the 80 km boundary layer, to an internal temperature of $\sim 1900K$. Below this boundary layer, the temperature increases slower until it reaches the bottom boundary layer, where it increases quickly again to the initial core mantle boundary (CMB) temperature (Figure 4a). The initial composition is homogeneous and changes with partial melting and eruptions (Rolf et al., 2018).

2.2.2 Rheology

The rheology used in the models is viscoplastic, material deforms purely viscously at stresses below a certain threshold, the yield stress. The viscosity is pressure- and highly temperature-dependent. The deformation mechanism is dislocation creep, not considering other mechanisms like diffusion creep. The rheology follows the Arrhenius law to account for these factors:

$$\eta(T, d) = \eta_0 \exp \left[\frac{E + Bd}{RT} - \frac{E}{RT_0} \right], \quad (1)$$

where T is absolute temperature, d is depth, E is activation energy, R is the gas constant and $B = E + pV$, where V is activation volume, which is dependent on the pressure p , g is the gravitational acceleration and ρ represents the density of the area of interest. η_0 is the viscosity at the reference pressure $p = 0$ and reference temperature T_0 (Armann and Tackley, 2012). The initial viscosity changes with depth is shown in Figure 4b. The reference viscosity for Venus is difficult to constrain, the value chosen here is 3×10^{20} MPa s, the value for Earth is in the range of $1 \times 10^{20} - 1 \times 10^{21}$ (Mitrovica and Forte, 2004).

Large viscosity contrasts are considered to enable the generation of a stagnant lid on top of the mantle. To produce global overturn events, the lithosphere must be weakened, the convective stresses must reach the yield stress (Van Heck and Tackley, 2008).

Viscoplastic yielding is employed, when the yield stress is reached, to make this possible (Moresi and Solomatov, 1998). The yield stress is varied throughout the cases to produce both stagnant and episodic lid cases and changes with depth following Byerlee's law:

$$YS = YS_0 + f \times P, \quad (2)$$

where YS_0 is the varied value for yield stress, P is pressure and $f = 0.2$ is the friction coefficient.

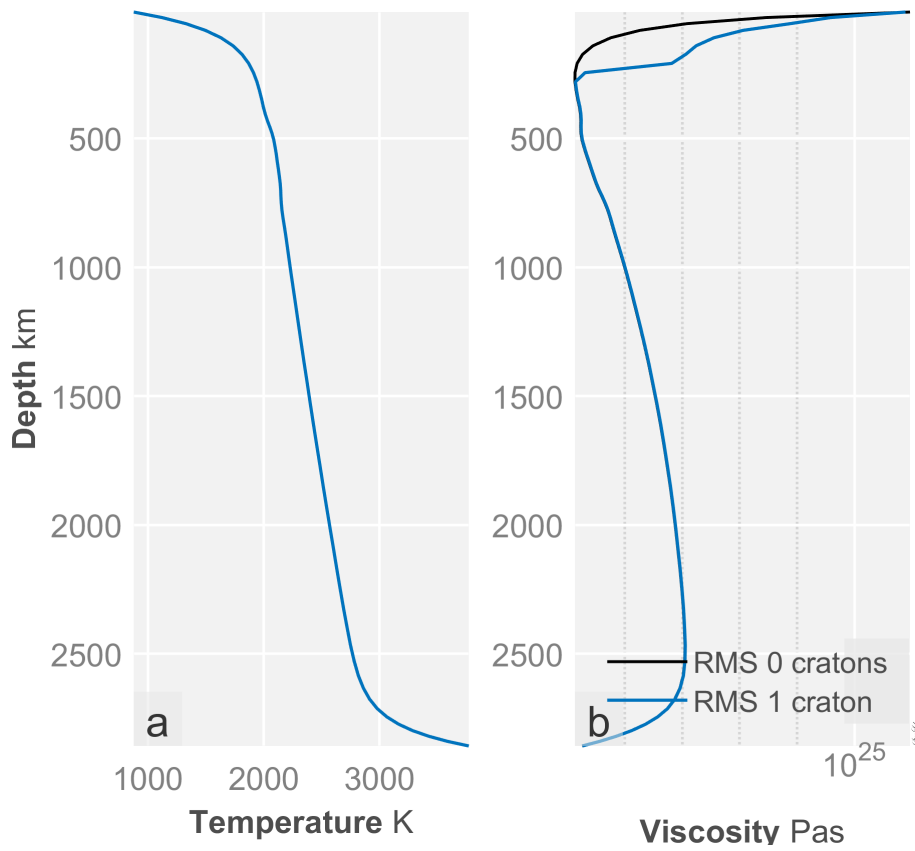


Figure 4: Initial root mean square (RMS) temperature and viscosity in the mantle, shown for a model with craton and a model without.

Mantle thickness	2866	km
Core radius	3186	km
Surface temperature	740	K
CMB temperature	3870	K
Gravitational acceleration	8.87	m/s ²
Craton thickness	231	km
Crustal thickness	25	km
Internal heating rate	5×10^{-12}	W/kg
Reference viscosity	3×10^{20}	Pa s
Activation energy	2×10^5	J/mol
Activation volume	3.5×10^{-6}	cm ³ /mol
Reference temperature	1613	K
Yield stress	10 ⁶ , 150, 100, 80, 40, 20	MPa
Number of cratons	0, 1, 2, 3, 4	

Table 1: Model parameters

2.2.3 Minerology

The initial composition of the mantle is 80% harzburgite, consisting of 25% pyroxene-garnet and 75% olivine, and 20% basalt, consisting of 100% pyroxene-garnet. The tracers track the composition between these two endmembers, which begins with a homogeneous composition and changes with time due to melting. The phase transitions are present in the model as these are important for the mantle flow patterns (Rolf et al., 2018). The minerals from the two different phase systems undergo phase changes at slightly different depth. On Venus, the phase transitions for the pyroxene-garnet system are situated at 65 km, 440 km and 800 km depth and the transitions for the olivine system are situated at 450 km and 730 km depth (Rolf et al., 2018). Because of the difference in gravitational acceleration between Venus and Earth, these transitions are proposed to be situated deeper in the Venus mantle than they are in Earth (Armann and Tackley, 2012).

2.2.4 Partial melting

The mantle composition in the model is initially homogeneous and changes with time by partial melting. The melting and eruptions in the model is greatly simplified, assuming

that the upper mantle is molten. When the local temperature reaches the solidus, the basaltic component melts. The melt is considered buoyant, therefore, when melting occurs, it rises quickly and is deposited on the surface as basaltic crust (Rolf et al., 2018). In reality, melt from the mantle may migrate towards the surface, but never reach it, forming intrusions. Partial melting and eruption of hot material is an important mechanism for cooling the planet, when global overturn events are absent (Turcotte, 1989). Eruption is generally possible on both cratonic and non-cratonic surfaces.

2.2.5 Pre-imposed cratons

As seen in models of the Earth (Rolf et al., 2012), imposed cratons have an impact on the internal dynamics of a planet. The proposal that Venus’ tesserae regions may be comparable to Earth’s cratons, makes it interesting to examine the effect of cratons on mantle dynamics in a different tectonic mode. The cratons are pre-imposed, meaning that they are in place at the initiation of the model. This is because the origin of cratons is unknown, which is also the case for Earth. The modelled cratons are highly simplified, Archean cratons, and are assumed to be units with different buoyancy and distinct material and rheological properties compared to the mantle. Each unit has a strong root and weaker crustal layer on top; they can thus be seen as an analogue to Earth’s continents, which also feature a strong Archean root and a weaker crustal layer. The density is generally the same for cratons and mantle. However, some of the cases experienced subduction of the cratons and this is not favourable when examining the impact of the cratons on the mantle. To prevent this the density contrast between the mantle and the cratons in these cases were changed from 0 to -20 kg/m^3 , making them less dense and more difficult to subduct.

The cratons imposed on the models cover a total of 10% of the surface. There are cases with one, two, three and four cratons of 10%, $2 \times 5\%$, $3 \times 3.33\%$ and $4 \times 2.5\%$ coverage. To reproduce the dynamics of a circular craton on 3D sphere, without modelling the 3D shell, the craton sizes are applied to the sphere and thereby adjusted for the 2D model. A cylindrical craton with a given radius is chosen to cover a certain fraction of the 3D sphere. The 2D model is essentially a cross section at the equator of the 3D sphere, so that the craton seems to cover a larger area in 2D than in 3D, this facilitates easier

comparison between 2D and 3D models. The conversion of craton size from 3D to 2D geometry follows this equation:

$$\frac{A}{A_T} = \frac{1}{2}[1 - \cos\alpha] \quad (3)$$

where A and A_T is the area of the craton are and the total area of the sphere. α is the angle of the craton radius from the centre of the planet. This angel is calculated for each of the craton sizes.

2.3 Diagnostics

The post-processing is done with StagLab, which is a MATLAB script developed to post process scientific data produced by the StagYY code in an easy and efficient way (Crameri, 2018). StagLab provides fully automated diagnostics, which are objective and in many ways better suited than the subjective diagnostics commonly performed by hand (or eye). Even though some of these automated diagnostics are still in development and could be further improved (see e.g. plume tracking in Section 3.4), they are useful for studying the results of the numerous models presented here.

- **Plume tracking:** The plumes in the mantle are tracked to gain insight into how they behave throughout the model time and how they are affected by imposed cratons. Slabs (cool plumes) are tracked because they may indicate the timing of global overturn events, a characteristic of Venus’ episodic style of lithospheric convection. When a slab is detected in the mantle, an overturn is ongoing. Hot and cold plumes are detected when their temperatures exceeds a certain threshold value. If $f_{hot} = 1$ anomalies are detected when they differ 100 % from the average temperature of the current depth level, closer to 0 the required difference decreases. The value chosen for the hot plumes is 0.45. It is chosen because it gives the best representation of the mantle plumes visible in the images. For cold plume recognition 0.4 is used.
- **Surface mobility:** Global overturns are also tracked by surface mobility. The surface mobility is calculated by the plate-core root mean square (RMS) horizontal velocity divided by the asthenosphere RMS velocity. In a stagnant lid model, the surface mobility is ~ 0 , whereas in a mobile lid model the surface mobility is typi-

cally > 1 . For an episodic lid model, the surface mobility will alternate between the two, when the value is > 1 an overturn is occurring, when the value is ~ 0 there is no overturn.

- **Crustal Thickness:** The crustal thickness is tracked to get insight into the crustal production and renewal of the surface, even when global overturns are absent. The crustal thickness is zero at the initiation of the models and increases through eruption of molten material in the upper mantle. When the temperature in a certain area exceeds the solidus, the basaltic component of the mantle will partially melt and erupt. This material is assumed to be buoyant and will immediately be emplaced on the surface and create basaltic crust. The cratons have a pre-imposed crustal layer, however this cratonic crust is not considered with the non-cratonic crust. The cratonic surfaces are therefore removed from the calculation of mean crustal thickness, because of their difference in crustal evolution.
- **Surface age:** The surface ages on Venus can to a certain extent be constrained from crater statistics and it is therefore interesting to compare to modelled surface ages. The surface age changes with eruptions and overturn episodes, like the crustal thickness. The cratonic surfaces are also removed from the mean surface age calculation.

2.3.1 Visualisation

The visualisation of all the results is done using state-of-the-art Scientific Colour Maps (Crameri, 2018). The colour maps are designed to prevent distortions of the underlying model data, make the figures intuitively readable through perceptual colour order, and do not exclude colour blind people.

3 Results

To get an insight into the relationship between cratons and mantle dynamics, models with varying number of cratons and yield stresses were set up. There are thirty cases in which the number of cratons is varied from zero to four and the yield stresses are set to 1×10^6 MPa (practically infinite), 150 MPa, 100 MPa, 80 MPa, 40 MPa and 20 MPa. The total surface coverage of cratons in each case is 10 %, and the cratons are equally distributed (Figure 5). The yield stresses are chosen to produce models with stagnant lid and episodic lid mantle convection.

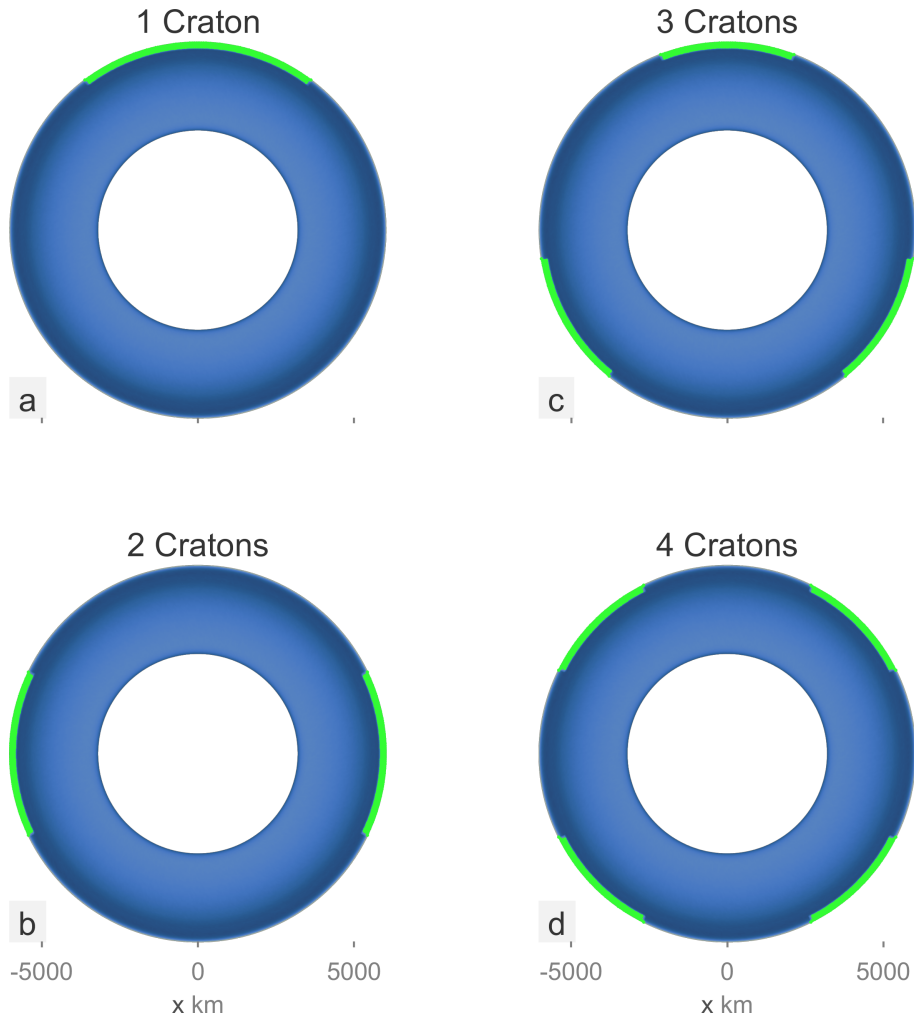


Figure 5: Initial distribution of cratons, marked in green, in cases with varying number of cratons.

The general evolution of a stagnant lid, reference case (Figure 6) shows an initially homogeneous mantle mixing and separating through time by partial melting and eruptions. The plumes are initiated at the core-mantle boundary after short time and the number of plumes decreases through time as the model evolves towards a steady state (Figure 6). The thermal evolution begins with a period of intense heating caused by the radiogenic heat production, then a steady state is reached after ~ 3 Gyr for most of the models (Section 3.3).

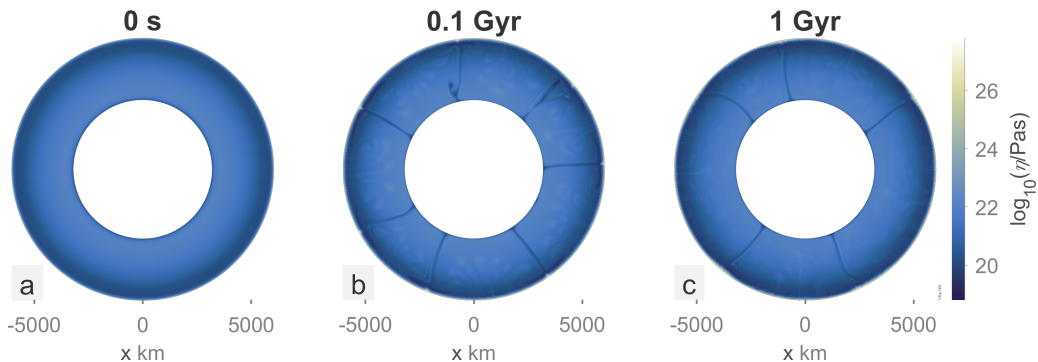


Figure 6: Viscosity evolution of the model with no cratons and infinite yield stress.

3.1 Overturn episodes

Episodic overturns are favoured by decreasing the yield stress (Rolf and Tackley, 2011), the exact yield stress at which overturns are initiated may also vary with the number of cratons on the surface. For cases with no cratons, overturn is achieved for yield stresses of 100 MPa and less. For cases with one craton they are achieved already at 150 MPa and less. For cases with two cratons, overturns occurs at 80 MPa and less and for three and four cratons only at 40 MPa (Table 2).

The total duration of overturns in the models also change with yield stress and imposed cratons, shown in the parenthesis in Table 2. For the cases with 100 MPa yield stress, the total overturn duration is the same for the two cases, zero and one craton. For 80 MPa, the duration is still similar for the zero and one craton cases, but lower for the two cratons case. For the 40 MPa models, the duration of overturn events is similar for all cases with cratons, but much higher for the cases without cratons. Comparing

these numbers with the number of overturns in the same table, the duration of a single overturn is much longer in the case with zero cratons and 40 MPa yield stress, than for the other cases with 40 MPa yield stress, having only three overturn episodes as opposed to six or seven. In the 20 MPa cases the zero craton case yields the closest to continuous subduction. The one craton case is the one with the longest quiescent periods.

	0 cratons	1 craton	2 cratons	3 cratons	4 cratons
Infinite	- (0)	- (0)	- (0)	- (0)	- (0)
150 MPa	- (0)	1 (0.015)	- (0)	- (0)	- (0)
100 MPa	2 (0.05)	2 (0.05)	- (0)	- (0)	- (0)
80 MPa	3 (0.08)	3 (0.09)	3 (0.04)	- (0)	- (0)
40 MPa	3 (0.51)	5 (0.25)	5 (0.28)	5 (0.22)	7 (0.23)
20 MPa	- (0.97)	- (0.79)	- (0.88)	- (0.81)	- (0.87)

Table 2: Overview of all models with different yield stresses and number of cratons. Red colour signifies stagnant lid, green colour signifies episodic lid and blue colour signifies continuous mobile lid. The number signify the number of overturns and total fractional time of overturns (1 = continuous subduction).

Two different approaches are used to determine the models’ tectonic mode: the number of slabs in the mantle and the surface mobility. In Figure 7 the two diagnostics are compared, showing that they detect the same overturn events, the main difference being that the number of slab diagnostic also gives some information on how many slabs are affecting the surface simultaneously and thereby at which spatial wavelength the overturn occurs. The number of slabs diagnostic is hereafter used to show the initiation time and duration of overturn events in all models.

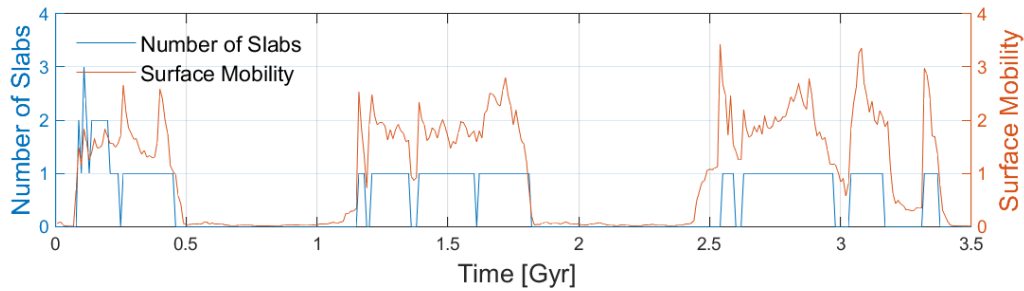


Figure 7: Example of number of slabs versus surface mobility as ways of tracking global overturns.

Plumes and slabs are detected automatically in StagLab. They are defined as hot or cold upwellings (plumes) or downwellings (slabs) in the mantle. They are detected as anomalies if their temperatures exceed a certain threshold (Cramer, 2018). For detection of slabs, this threshold is set to 0.4 as explained in Section 2.3, however, the same slab is recognisable with threshold values ranging from 0.3 to 0.7. The detection of a slab is illustrated in Figure 8. The occurrence of slabs show when the model is experiencing subduction (Figure 9). For the cases with high yield stress, there is no subduction and therefore no slabs. Examining the number of slabs through time gives a representation of when overturns occur and gives an indication of how it happens in terms of the number and duration of subduction events. Figure 9 shows the number of upper mantle slabs, to get the best representation of the starting time of the events.

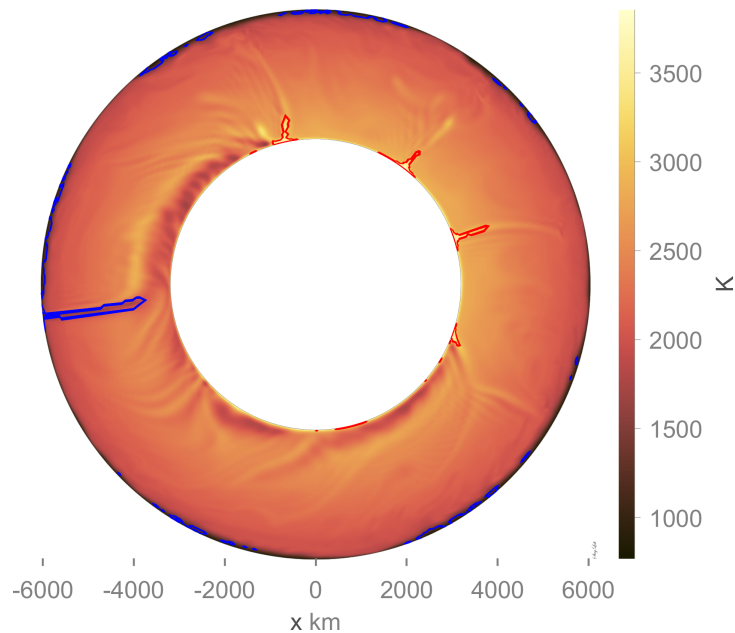


Figure 8: Detection of a slab in the case without cratons and with 40 MPa yield stress shown in a temperature field, slabs are marked with blue, plumes are marked with red

Cases with subduction are produced by decreasing the yield stress, but the exact yield stress that favours subduction changes with the number of cratons. For cases without cratons (Figure 9a), subduction happens when yield stress is decreased to 100 MPa. At this yield stress subduction starts at ~ 2.54 Gyr, then there is another subducting slab a short time later, both of them last for ~ 50 Myr. The second period of subduction happens

at ~ 3.34 Gyr and lasts ~ 70 Myr. The quiescent period in between the two subduction periods lasts ~ 670 Myr. For the case with 80 MPa yield stress, the subduction periods start earlier, at ~ 1.5 Gyr. In this case there are four distinct periods with subduction lasting ~ 270 Myr, ~ 400 Myr, ~ 500 Myr and > 210 Myr. For the case with 40 MPa yield stress, there are three distinct periods of subduction. These last longer than in the previous cases, ~ 390 Myr, ~ 680 Myr and ~ 840 Myr. The quiescent periods are also more distinct, but last approximately as long as for the higher yield stress cases. The 20 MPa case shows close to mobile lid convection, with only short quiescent periods and mostly continuous subduction. This case also has more subducting slabs simultaneously.

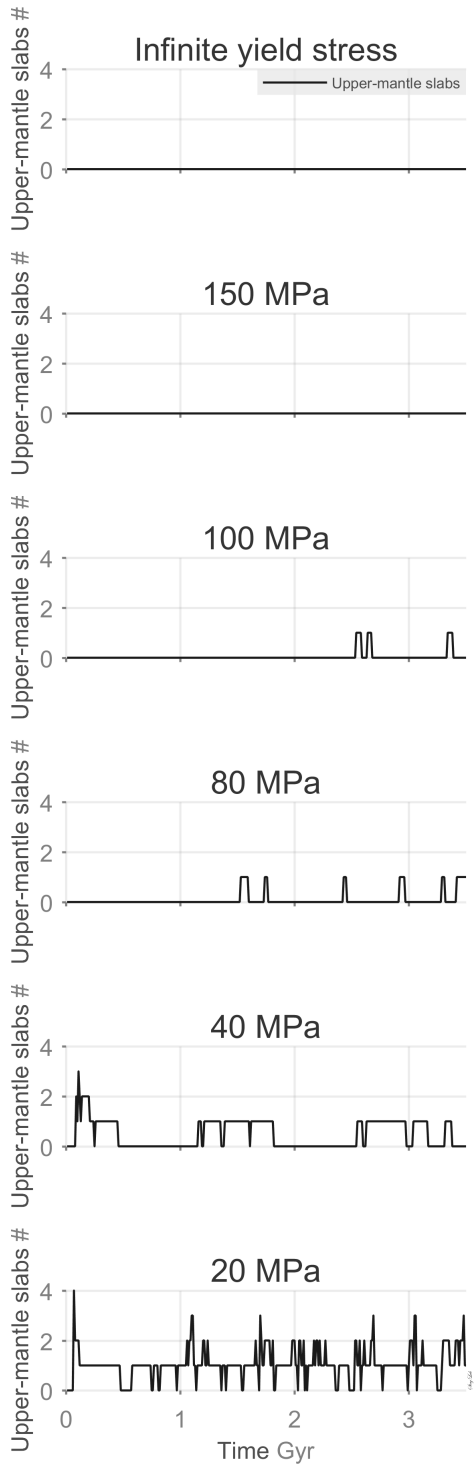
For the cases with one craton (Figure 9b), the subduction is initiated only at higher yield stress. There is one subduction period in the model with 150 MPa at ~ 2.5 Gyr. For the lower yield stresses, the subduction is initiated at an earlier time. The quiescent periods are longer and the subduction periods are more distinct than for cases without cratons. The case with yield stress of 40 MPa has five subduction periods. These are shorter than the ones for no cratons, but the quiescent periods are approximately the same length. The 20 MPa case starts out with two quite distinct subduction periods with quiescent periods in between. At ~ 1.5 Gyr it changes into more continuous subduction, with close to no quiescent periods.

The cases with two cratons does not have any subduction before the yield stress is decreased to 80 MPa (Figure 9c). The first subduction starts at 1.2 Gyr and there are three subduction periods in total. The quiescent periods are longer than the ones for no cratons (~ 1.3 Gyr and ~ 0.72 Gyr) For the case with 40 MPa yield stress there are also five subduction periods, these are very distinct and consist of one or two subducting slabs. The quiescent periods have approximately the same length as the ones in the one craton case. The 20 MPa case shows continuous subduction with only one quiescent period at ~ 2.5 Gyr, lasting ~ 250 Myr.

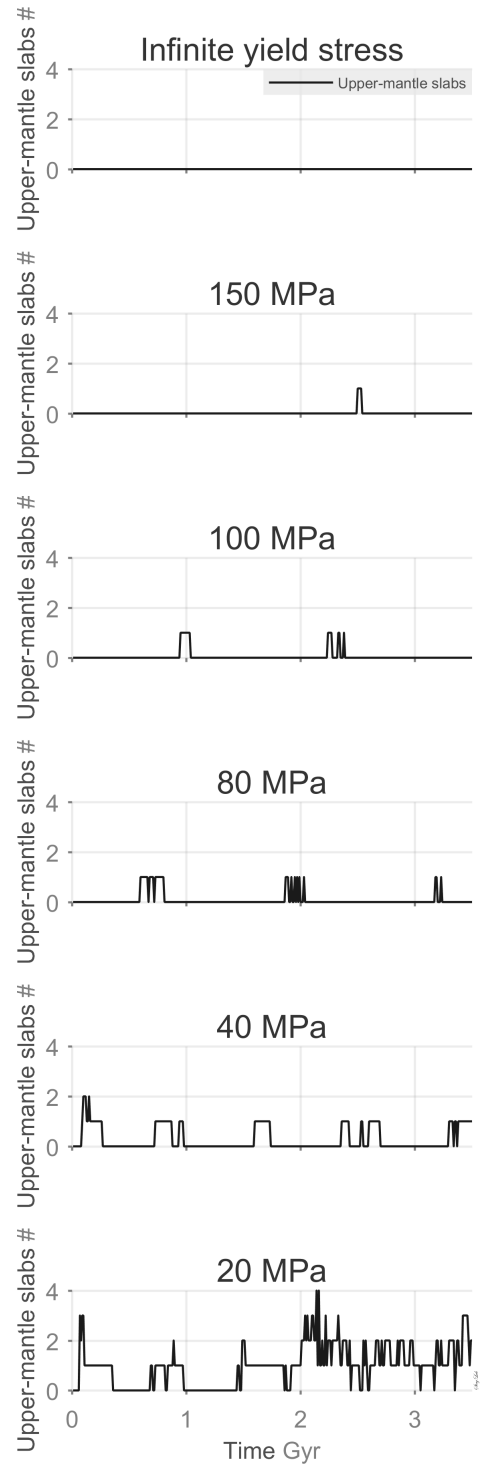
For the cases with three cratons, there is only subduction when the yield stress has been reduced to 40 MPa (Figure 9d). In this case the subduction periods are less distinct than for the previous cases. There are shorter quiescent periods and the duration of the

individual subduction periods are more difficult to distinguish. The 20 MPa case shows almost continuous subduction, with some quiescent periods, although these are very short.

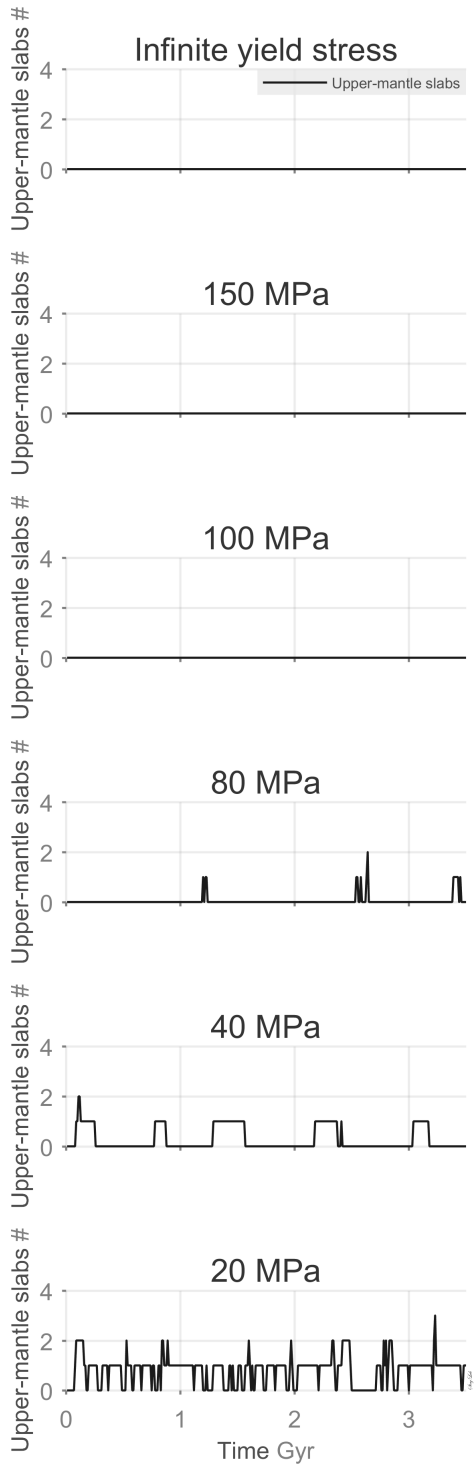
The cases with four cratons are quite similar to the three craton cases, although the quiescent periods in the 40 MPa case is longer and the subduction periods shorter (Figure 9e). In the 20 MPa case there are six or seven periods of subduction. This case shows a slightly higher number of slabs than the three cratons case.



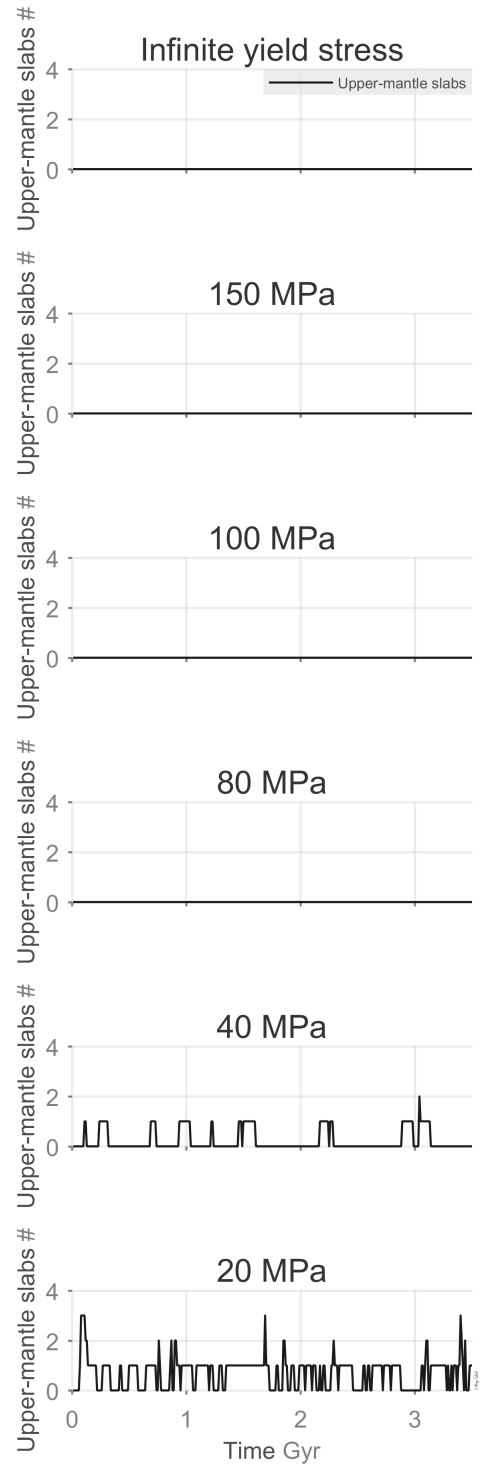
(a) 0 cratons



(b) 1 craton



(c) 2 cratons



(d) 3 cratons

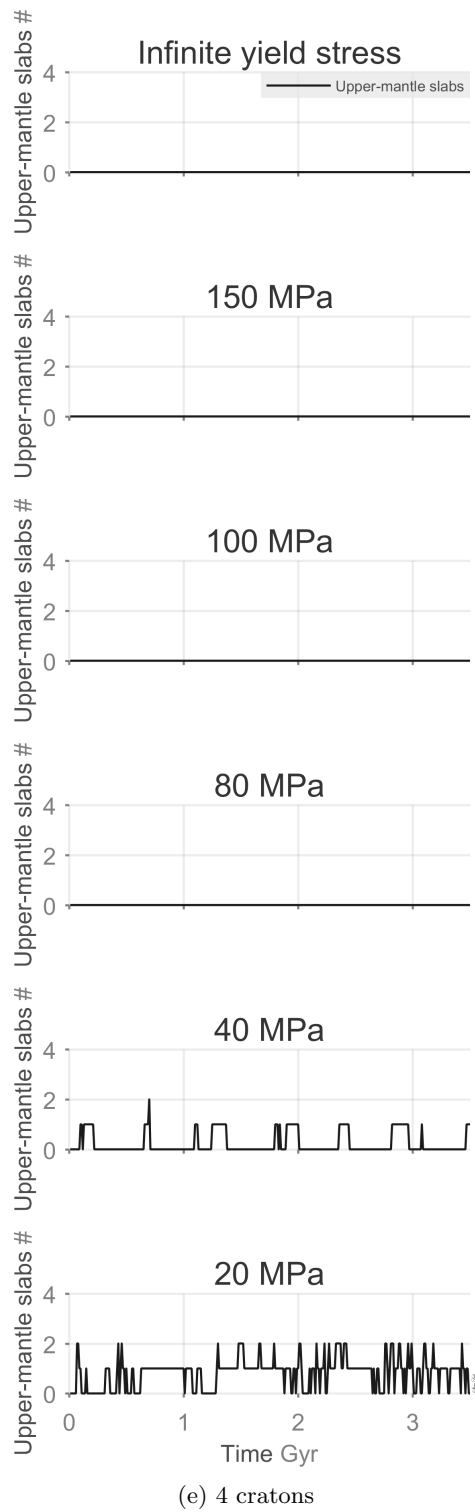


Figure 9: Number of upper-mantle slabs per time for models with varying number of cratons and yield stress.

3.2 Mode of overturns

The overturns are generally initiated on the opposite hemisphere from that containing cratons, or as far away from the craton as possible. Spreading ridges are often recognisable close to the cratons, on the opposite hemisphere to the subduction initiation. When overturn is initiated in cases with more than one craton, the subduction forces the cratons to collide and thereafter stick together for the remainder of the simulation. This is most likely caused by the model itself, since the tesserae regions on Venus are not clustered (Ivanov and Head, 2011) and our observations from Earth suggests that continents may collide and break apart again (Buiter and Torsvik, 2014).

The overturn episode takes place when one or several slabs subduct. For yield stresses of 80 MPa and higher, the slabs do not appear simultaneously, but straight after one another or with a small time gap. Figure 10 shows an overturn episode consisting of two slabs, one after the other, in a model with no cratons. The subduction disturbs the plumes visible in Figure 10a. This is the first overturn in this model and the plumes do not return to their original stability for the remainder of the simulation. A spreading centre is formed close to right side of one of the plumes, visible as an area of thinner crust marked with a circle (Figure 10a), and the subduction is then initiated in the opposite hemisphere, seen as a subduction slab (Figure 10b). At the time of the second subducting slab, the rifting is difficult to determine from this plot, because of the uneven crustal thickness caused by the previous slab. Diagnostics showing surface velocities could be used to better indicate the spreading centres.

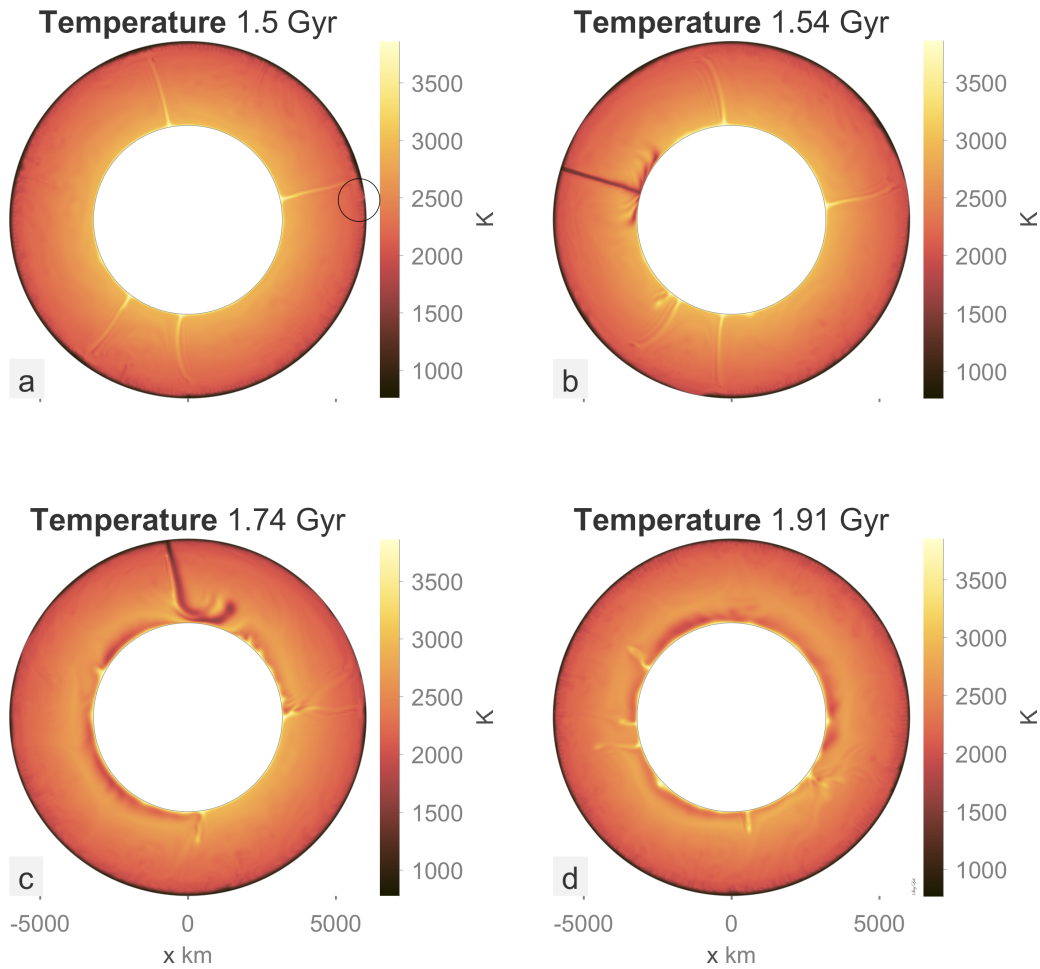


Figure 10: Temperature field showing an overturn event in the model with no cratons and 80 MPa yield stress. The overturn event consists of two subducting slabs following each other in time. The first is initiated at 1.54 Gyr and the other at 1.74 Gyr. The spreading centre is indicated by a circle.

An example of an overturn event in a model with one craton is shown in Figure 11. In this case the overturn is also initiated on the opposite hemisphere to that of the craton (Figure 11a). A spreading ridge is initiated to the right of the craton (Figure 12b), before subduction begins in the opposite hemisphere. Looking at the horizontal velocity (Figure 12), the first time step shows movement towards the underside of the craton and a upwelling there. In the next time step, the mantle has divided into only two convection cells and a downwelling has been initiated at the opposite side from the upwelling under the craton. The slab drags large parts of the surface down to the core-mantle boundary.

The craton is dragged towards the area of the slab and the downwelling stops when the craton meets the slab (Figure 11b). A rather long time passes before the plumes in the mantle returns to their original state. In between 0.8 and 1.4 Gyr, there are no plumes reaching the surface (Figure 11b, c and d).

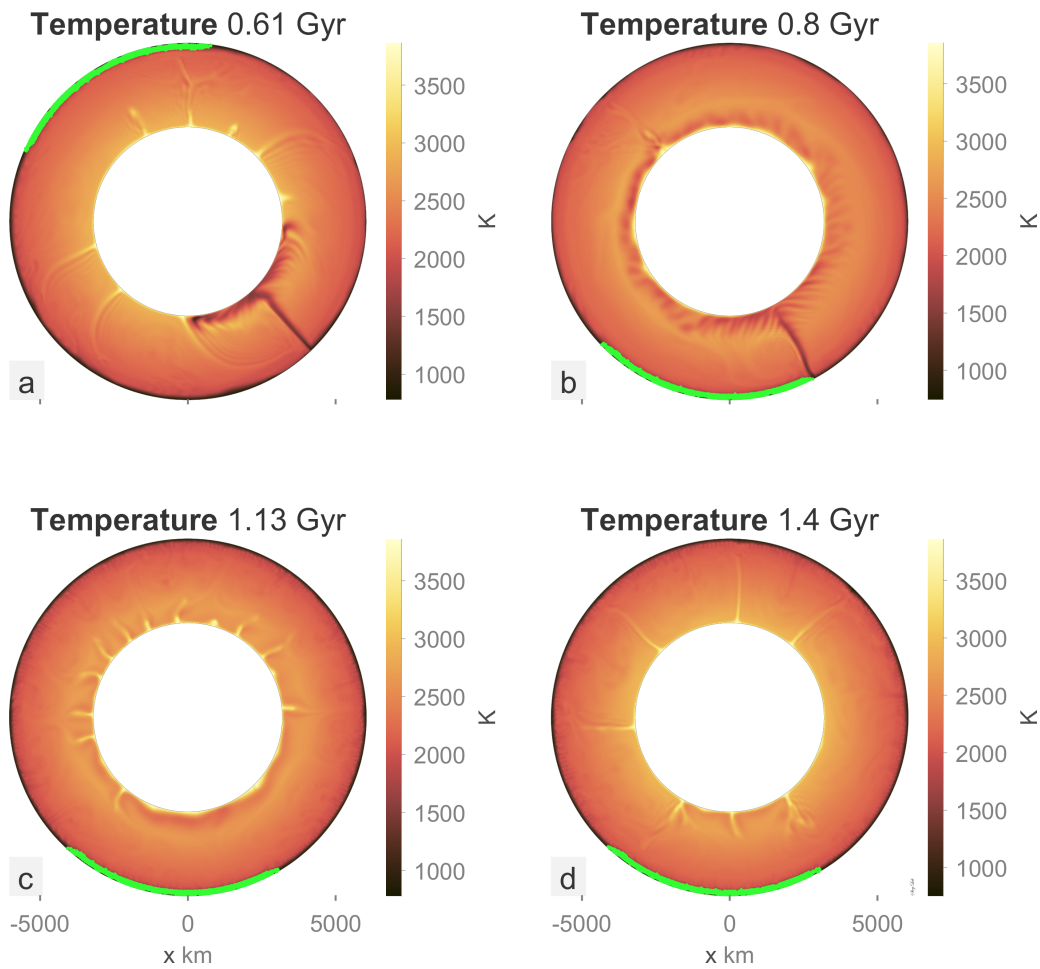


Figure 11: Temperature field showing the evolution of an overturn event in the model with one craton and 80 MPa yield stress. The craton is marked with green colour

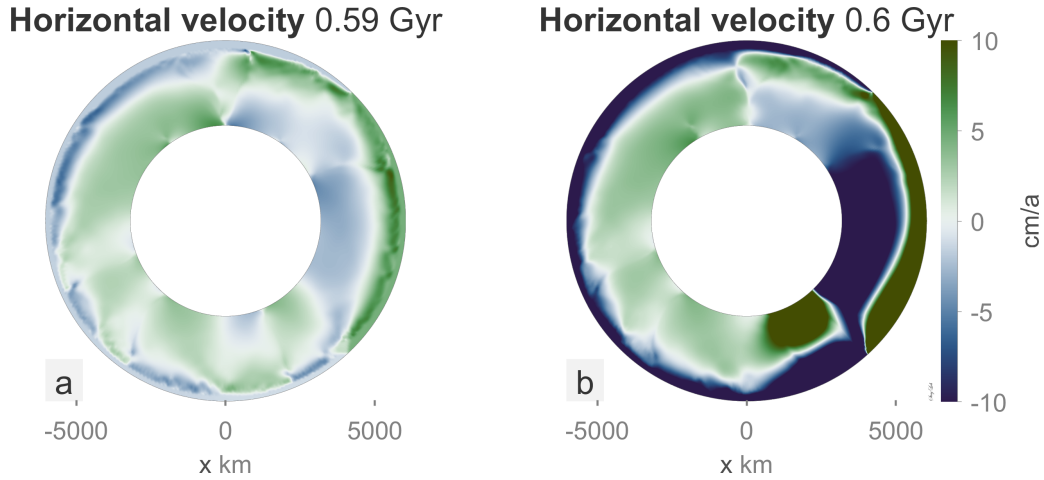


Figure 12: Horizontal velocity for the same case as Figure 11. Green colour is clockwise motion and blue is counter clockwise motion.

In the case with two cratons, the overturn that is shown in Figure 13 is not the first experienced in this model, the cratons are no longer equally spaced and have moved towards each other. This overturn was initiated in between the cratons, on the side where the distance between them is greatest (Figure 13a), causing them to move in the opposite direction to their initial movement. The cratons are dragged towards each other, until one of them reaches the subduction zone (Figure 13b). The subduction is cut off, but the cratons continue to move towards each other until they collide, squeezing the remainder of the surface down into the mantle (figure 13c). The cratons now stick together.

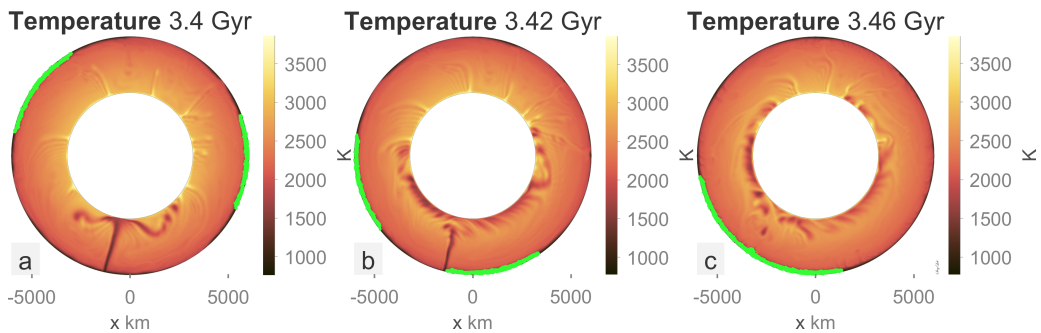


Figure 13: Overturn event in the case with two cratons and 80 MPa yield stress, shown in a temperature field plot.

For cases with three and four cratons and overturn events, the cratons will collide and stick together for the remainder of the modelling time (figure 14). Again, the subduction

is initiated where the distance between the cratons is greatest (figure 14a). In this case, only two of the cratons are moved and collide near the initiation point of the subduction (figure 14b). The third craton stays stationary because there are initiated spreading centres on both sides of the craton, marked in 14a with circles. Figure 14c shows the collision of the two connected cratons with the last craton, this happens already at 1.23 Gyr, and from this time onward the cratons will move together as one.

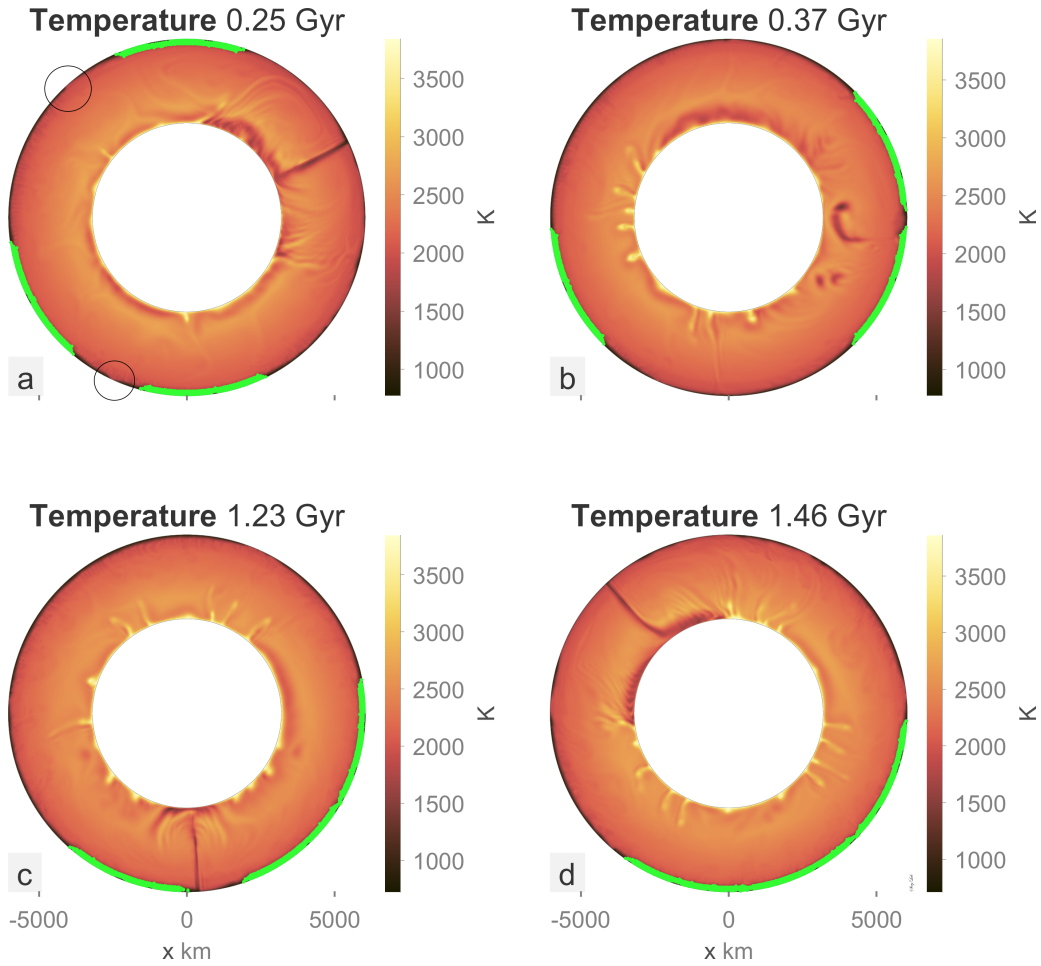
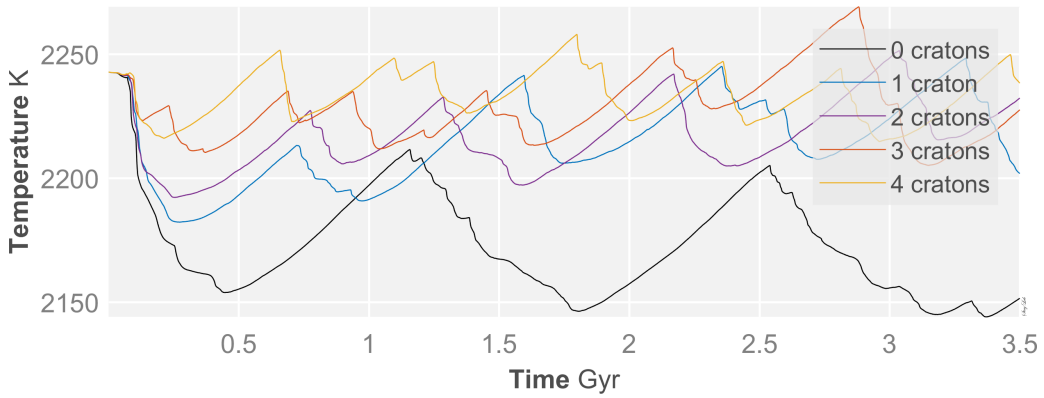


Figure 14: Overturn and craton collision in model with three cratons and 40 MPa yield stress. Circles in a. mark spreading centres.

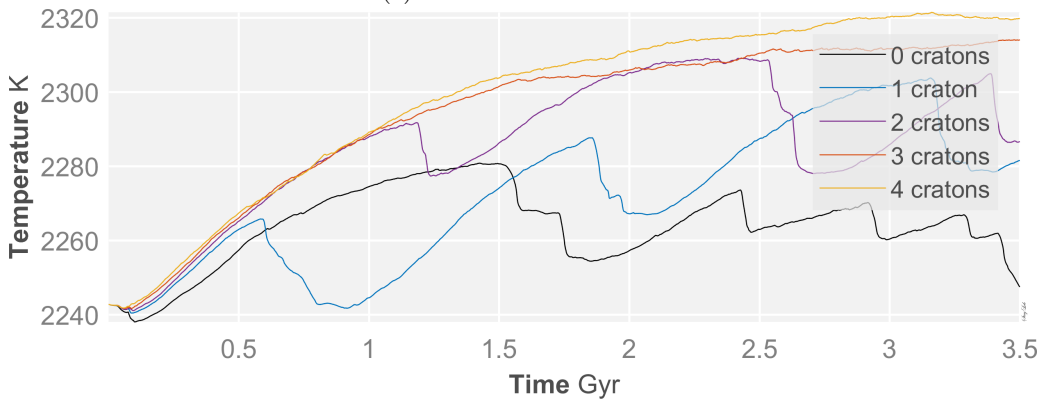
3.3 Thermal evolution

The initial mean mantle temperature in all models is $\sim 2240\text{K}$. When there are no overturns in the mantle, this temperature increases to $\sim 2320\text{K}$, if overturns are present, the

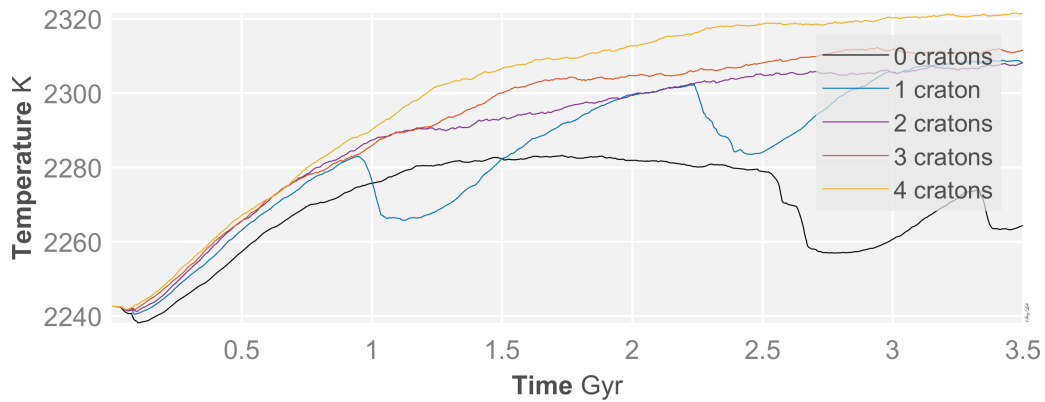
temperature will decrease depending on the number of overturns. The temperature evolution depends on both yield stress and number of cratons. The most prominent tendencies are that the temperature is lowest when there are no cratons and then increase when cratons are imposed and that the subduction periods cause the temperature to decrease drastically (Figure 15). The cases without overturn events will reach equilibrium after a certain time, because of the constant internal heating in the models. Figure 15e shows that the temperature of the case with one craton and infinite yield stress might not yet have reached equilibrium and may continue to rise. Drastic drops in temperature can be correlated with the overturns in Figures 9 and 7, showing the overturn events.



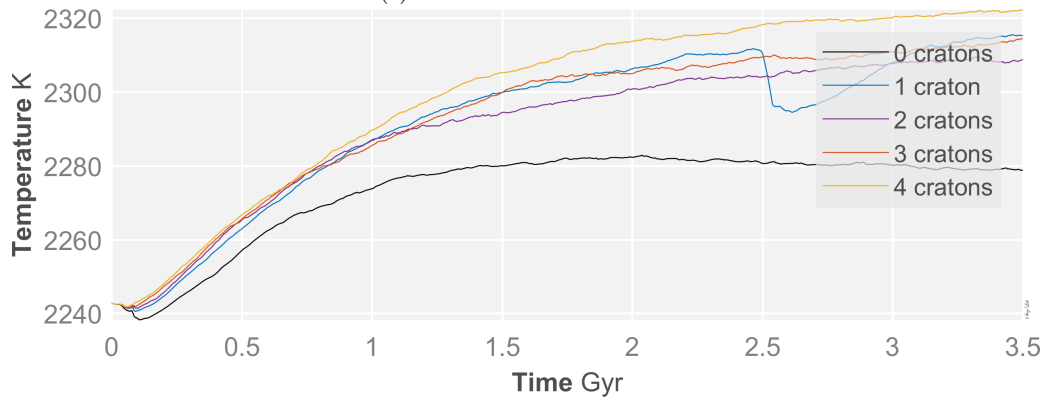
(a) Yield stress = 40 MPa



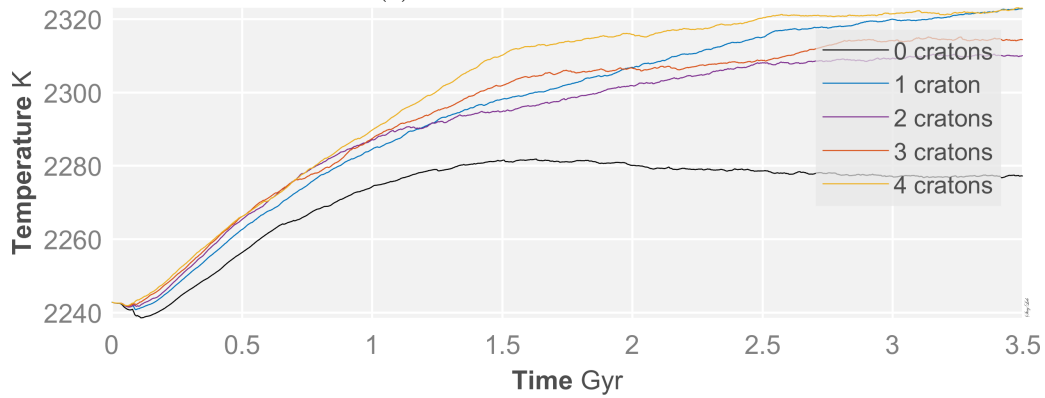
(b) Yield stress = 80 MPa



(c) Yield stress = 100 MPa



(d) Yield stress = 150 MPa

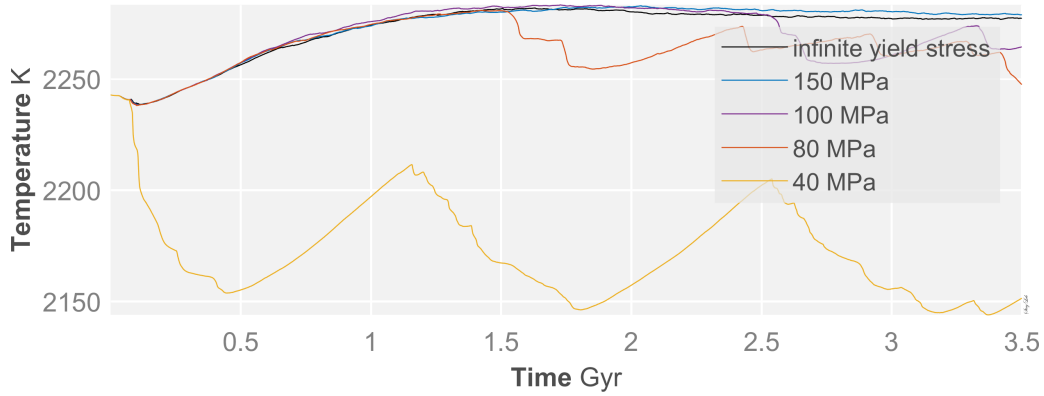


(e) Yield stress = infinite

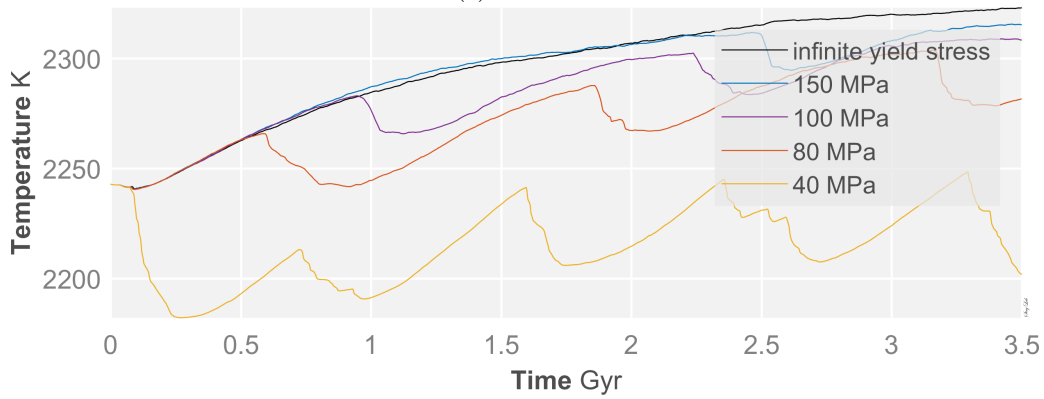
Figure 15: Mean mantle temperature through time, cases with the same yield stress are shown in each panel.

Comparing the temperature evolution for models with the same number of cratons but different yield stresses shows that unless there is an overturn event, the temperature varies

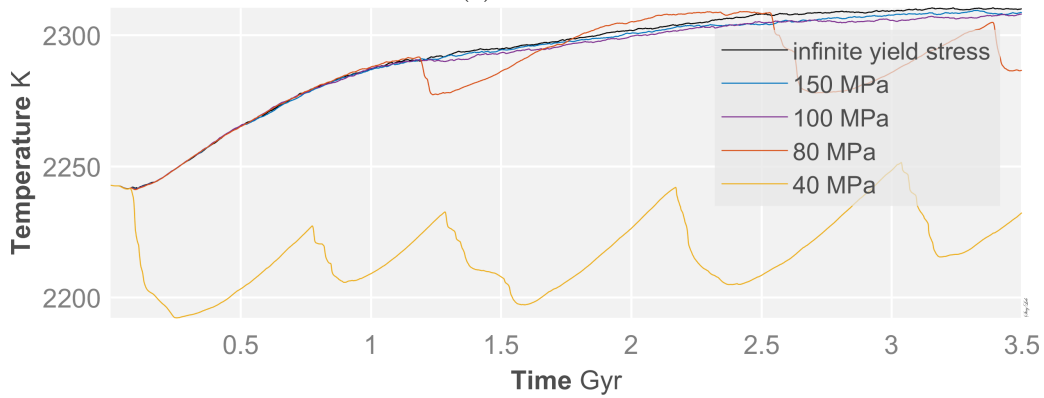
little (figure 16). When an overturn is present in the model the temperature drastically decreases. The more overturn events there are in the model, the lower temperature it has at the end of the model runs.



(a) 0 cratons



(b) 1 craton



(c) 2 cratons

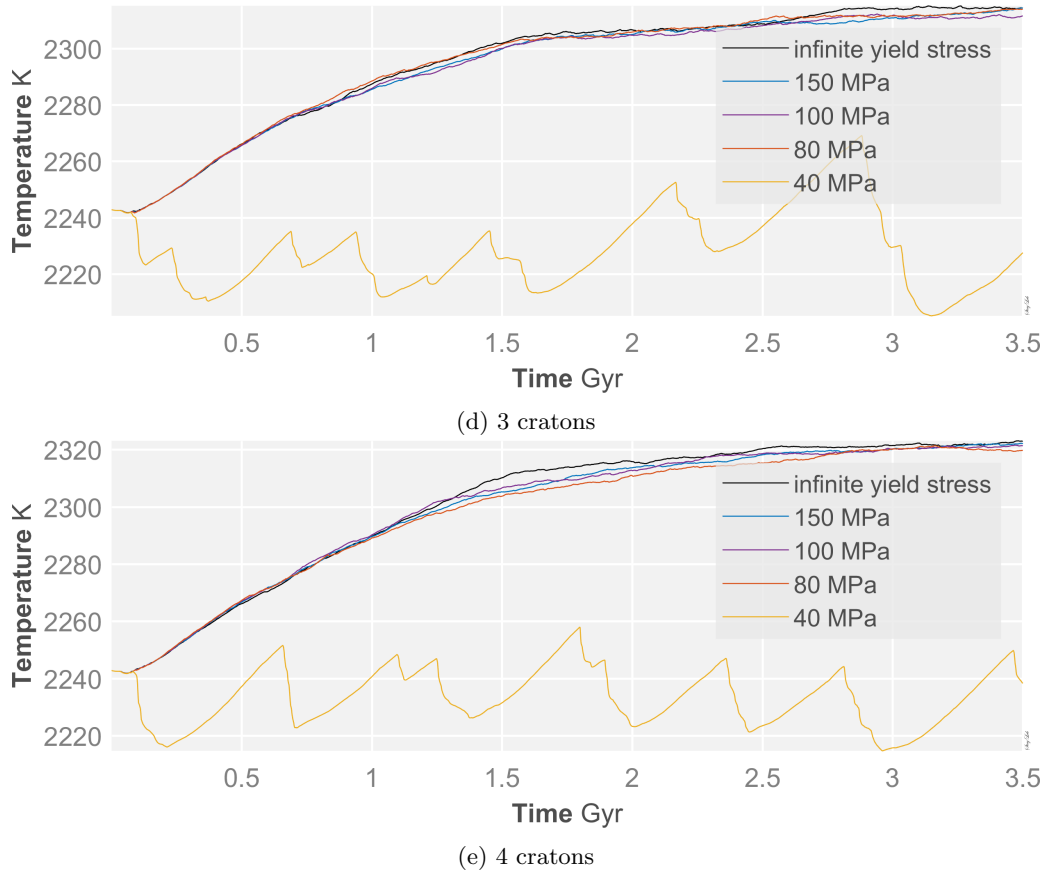


Figure 16: Mean mantle temperature through time with the same number of cratons.

3.4 Plumes

Plumes are detected by the same method as slabs, by detection of thermal anomalies in the mantle. There are certain other thermal anomalies that are also detected as plumes, though they are not traced from the CMB to the top boundary layer, and therefore are not considered to be plumes (Figure 17). This causes the number of hot thermal anomalies to lie around 10, when the model is not experiencing subduction. Instead of plotting all plumes, the plume detection is limited to only the ones found at mid-mantle depth (Figure 18). This provides a better picture of the plumes that may reach the surface and eliminate some of the thermal anomalies that are not plumes. However, Figure 18 shows that there are near to no plumes registered in the 40 MPa cases and the cases with one craton, which may be caused by the plume detection and actually signify disturbance of

plumes, rather than disappearance. There is also a drastic drop in number of mid-mantle plumes when an overturn is initiated for most models.

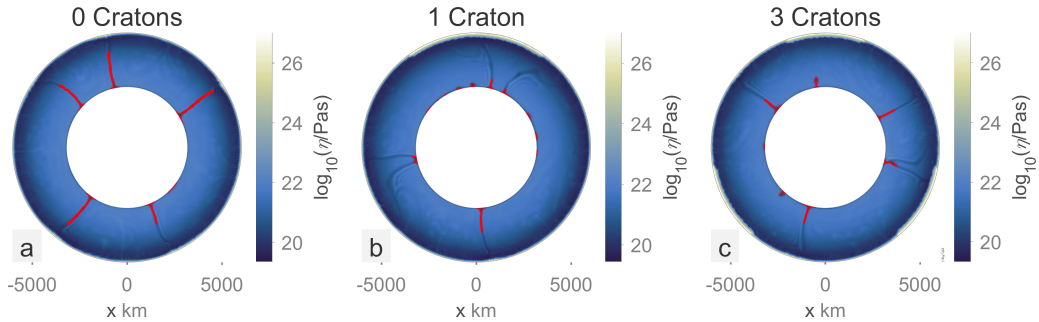


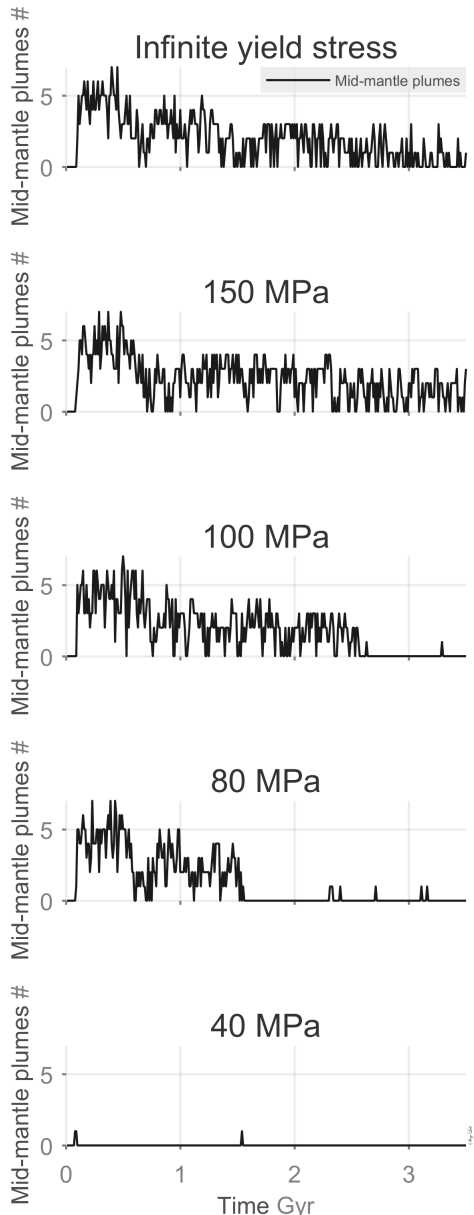
Figure 17: Viscosity plot showing detected plumes and other hot thermal anomalies for modes with zero, one and three cratons.

The number of plumes changes depending on the yield stress and the number of cratons. For the case with one craton, the number of mid-mantle plumes decreases through time from ~ 7 to ~ 3 (Figure 18a). The decrease in the number of plumes signifies an increase in convection cell size, meaning that the model may not yet have reached an equilibrium, since the number of plumes is still decreasing. In the cases with yield stresses of 100 and 80 MPa, the number suddenly drops to zero when there is an overturn event. In the case with 40 MPa yield stress, there are almost no plumes in the mid-mantle at all. The drastic drops in mantle plumes during and after global overturns may be due to the effect the subducting slabs has on the mantle. When the cool material is subducted down to the CMB, and cover it, the plume pattern gets disrupted and does not revert to its pre-overturn pattern in a long time. For the models with frequent overturns, the pattern of plumes never gets properly established in the first place, causing few or no detectable plumes.

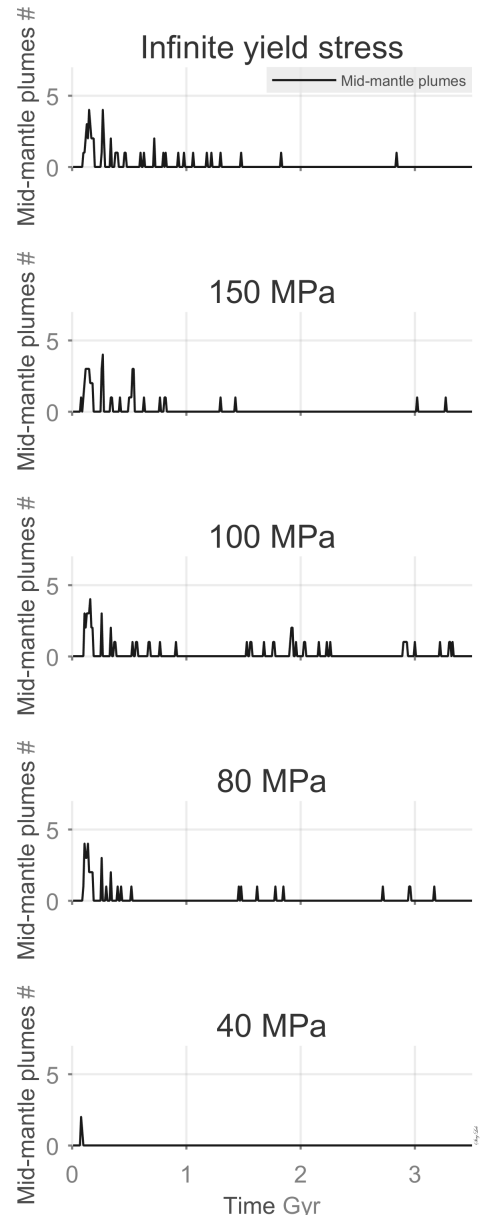
In the case with one craton, there is a generally low number of mid-mantle plumes (Figure 18b). In the case with infinite yield stress, the plumes disappear almost completely at ~ 1.75 Gyr. This disappearance of plumes cannot be correlated with an overturn event, since there are none. Figure 19 shows the evolution of the case with infinite yield stress and one craton. The two first panels show plumes on the opposite hemisphere to the craton. In Figure 19a there are three such plumes and in Figure 19b there is one. At these time steps plumes pointing towards the craton are also detected. In the last two

plots (Figure 19c and d) all plumes are pointing towards the craton and they are not detected by the plume detecting algorithm, even though they are visible in the plots.

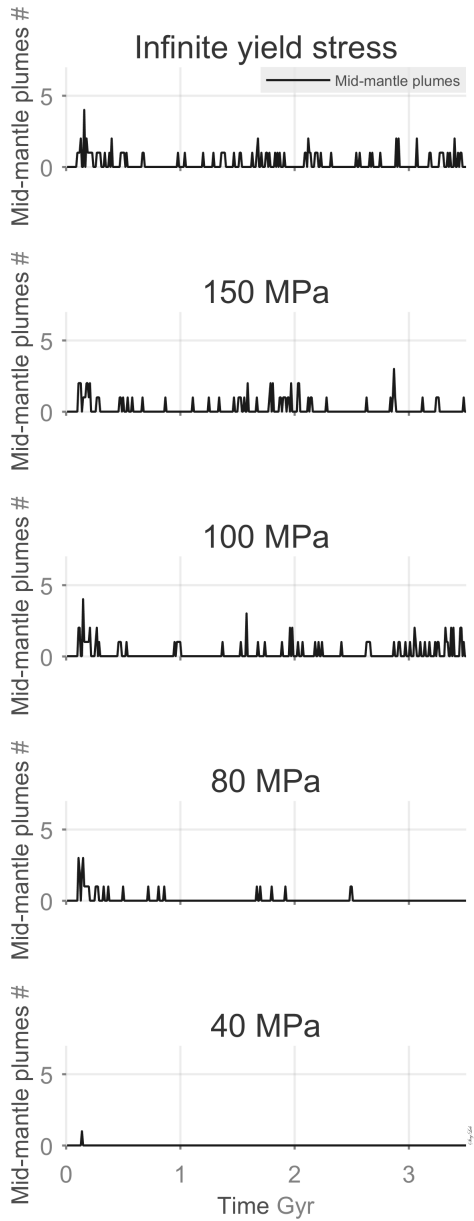
In the cases with two cratons, there are more plumes than in the zero craton cases (Figure 18c). For the case with 80 MPa, the absence of plumes can also be correlated with the overturn events. The cases with three and four cratons only have overturn events for yield stress of 40 and 20 MPa. The 40 MPa cases only have one mid-mantle plume at the start of the model (Figures 18d and 18e). There is generally a slight increase in plumes for all yield stresses without overturns for the cases with three and four cratons.



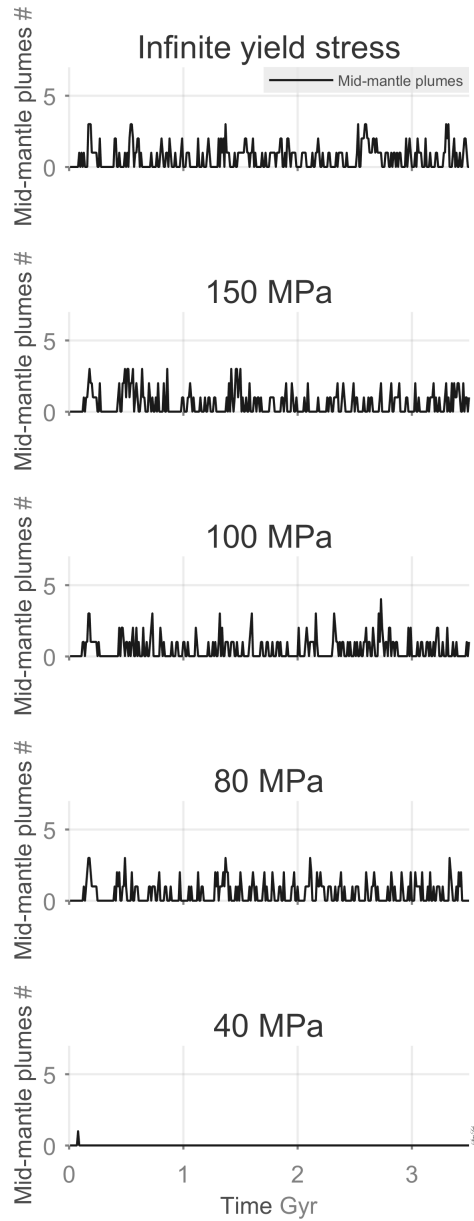
(a) 0 cratons



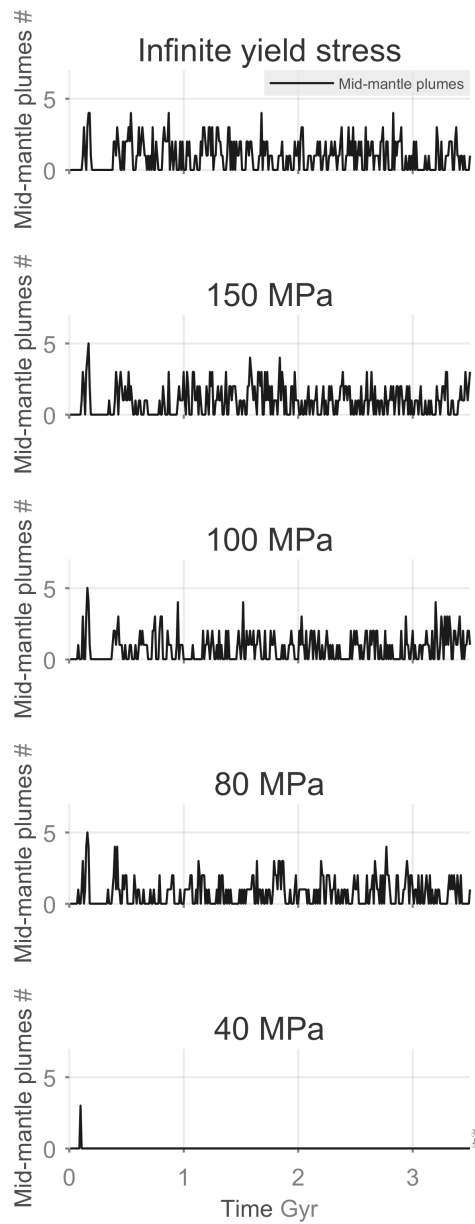
(b) 1 craton



(c) 2 cratons



(d) 3 cratons



(e) 4 cratons

Figure 18: Number of plumes at mid-mantle depth.

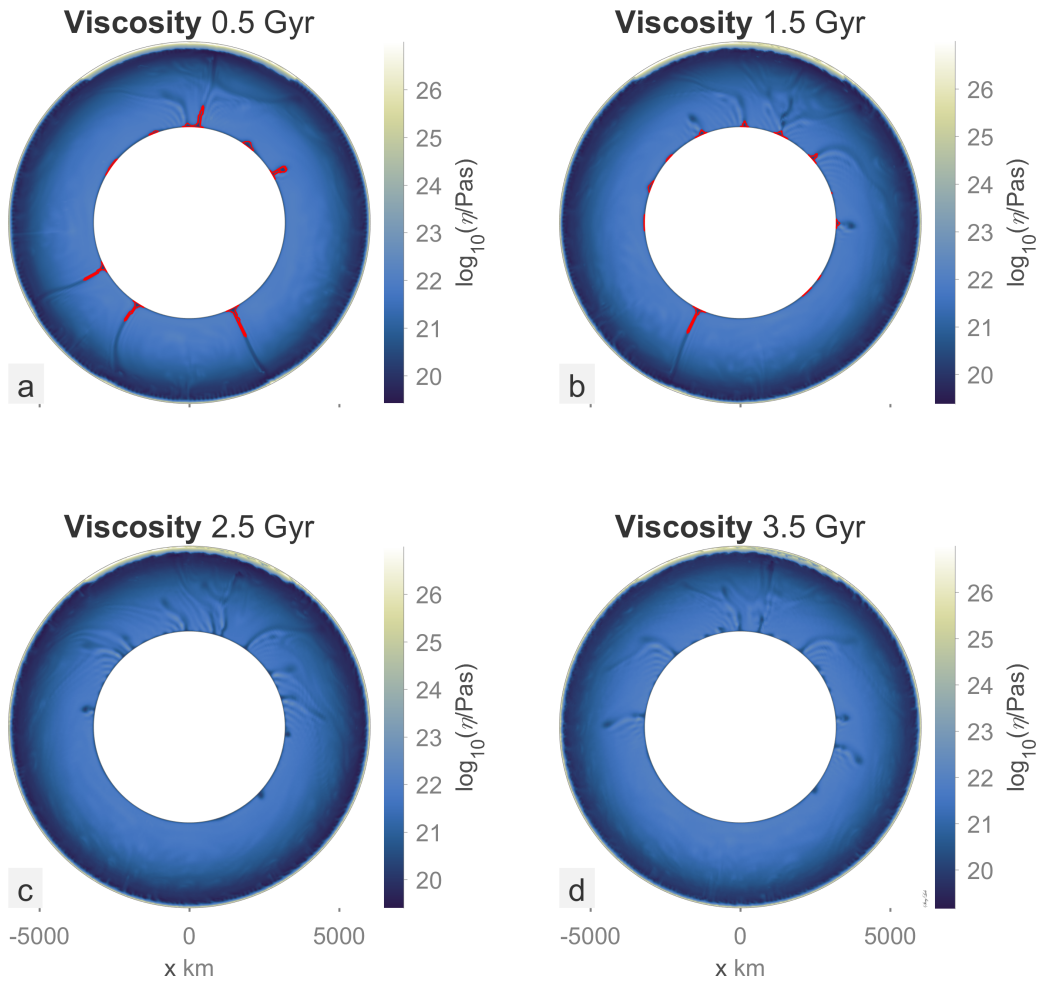


Figure 19: Four snapshots of the model with one craton and infinite yield stress, showing registered plumes and non-registered plumes.

The difference in number of plumes in the different models may be due to additional movement in the mantle. The mantle flow in the cases with infinite yield stress and different number of cratons show different convection patterns (Figure 20). Initially, the case with zero cratons has 11 convection cells, this is the highest number of all the models. This number is reduced to four during the simulation. In the case with one craton, the convection cells are initially quite unequal in size. There is one large cell on each side of the craton and several smaller cells in the opposite hemisphere. The smaller convection cells disappear further along in the simulation, leaving this case with only two convection cells. The cases with two, three and four cratons generally have four, six and eight

convection cells, respectively. The number may fluctuate a little through time, as seen in Figure 20c, where there are more than four convection cells at this specific time step. Even though the correlation between the number of convection cells and imposed cratons is not completely stable throughout the models, the general tendencies of a factor of two remains at least in the 2D cases.

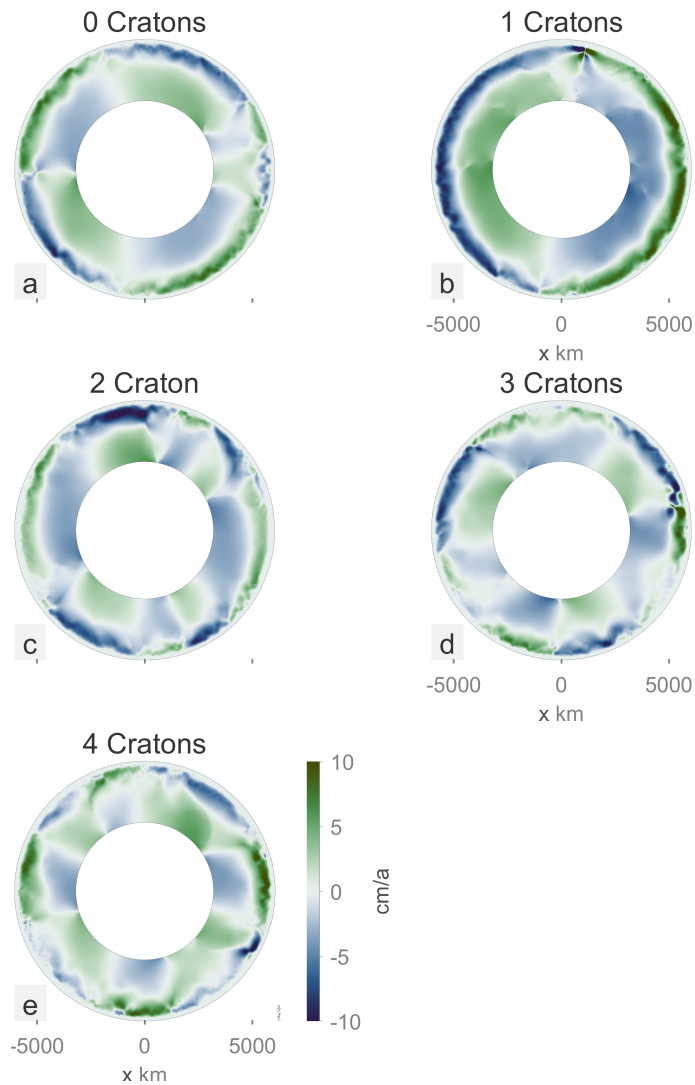


Figure 20: Horizontal velocity at 3.5 Gyr, for all cases with infinite yield stress, showing the correlation between number of cratons and number of convection cells. Green colour signifies clockwise movement, blue is counter clockwise.

A closer look at the cases with zero and one craton, shows the impact of a craton on the

plume movement (Figure 21). Both these are stagnant lid cases of infinite yield stress. For the case without cratons, the plumes are rather straight and stable, whereas the case with one craton shows plumes bending away from the craton. The horizontal and radial velocity plots show the impact of the craton on the movement in the mantle. Where the zero craton case has several convection cells, the one craton case only has two. The radial velocity in the plumes is also much higher in the cases without cratons than in the case with one craton.

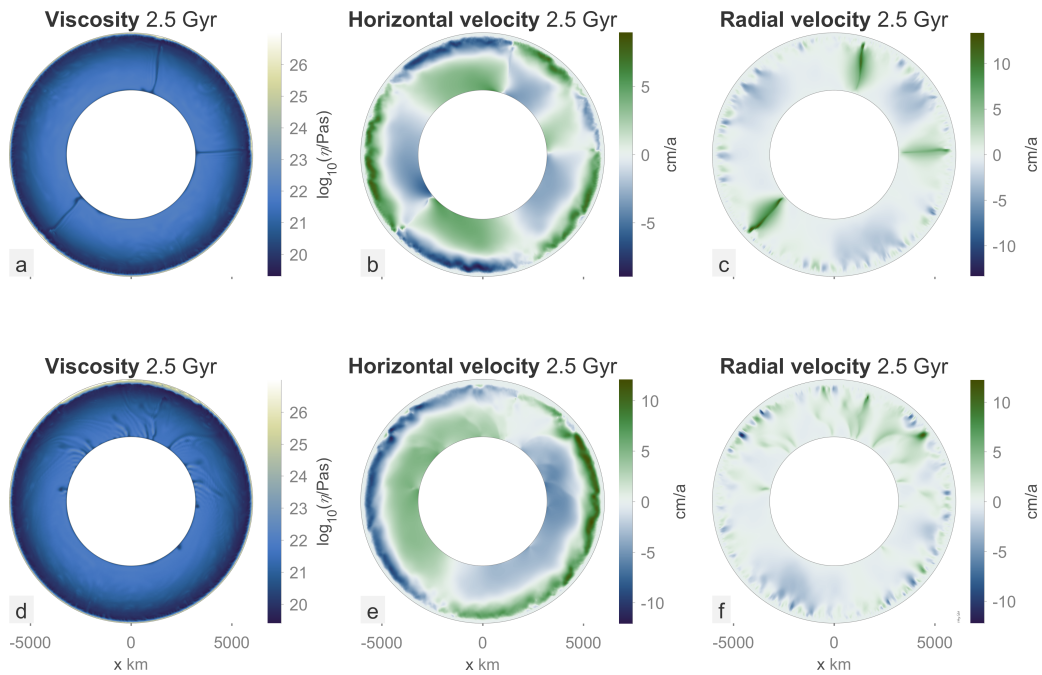


Figure 21: a, b and c show viscosity, horizontal and radial velocity for the model with infinite yield stress and no cratons, d, e and f show the same for the model with infinite yield stress and one craton. In b and e, blue colour signifies counter clockwise movement and green colour signifies clockwise movement.

3.5 Crustal thickness

The crustal thickness discussed here is chosen to be the thickness of the crust that is produced by melting and eruption on the surface that initiates at 0 km and grows through time. The cratonic crust, on the cratons, is pre-imposed and does not change with time. However, there are only a small amount of eruption on the cratons, owing to their thickness and the thickness of the thermal boundary layer, inhibiting eruptions. Therefore, cratonic crustal thickness appears in the following figures with much lower values than the non-cratonic areas (Figure 22).

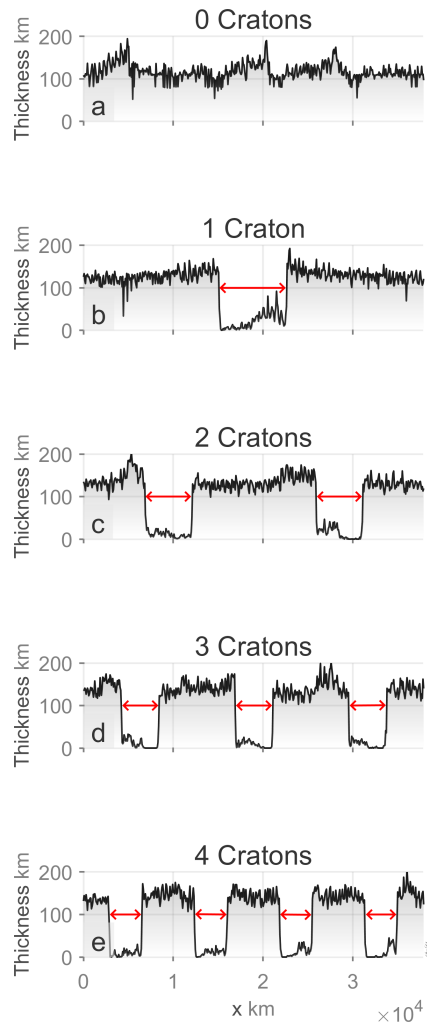


Figure 22: Crustal thickness for models with infinite yield stress and different number of cratons, the position of the cratons is indicated by red arrows.

For cases that yield overturn events, the crustal thickness depends on the timing of these events. The crustal thickness will increase with time and then drastically decrease when the overturn events are initiated. Figure 23 shows the crustal thickness right before and right after an overturn event. It is visible that the crustal thickness decreases, although there are areas at the edges of the craton that retain their thicker crust even after the overturn. The dip in crustal thickness at ~ 24000 km (Figure 23a) shows a spreading ridge (Figure 24). The overturn is initiated at the opposite side of the planet from this ridge. During the overturn episode, the craton moves towards the subduction site, and when they make contact, the subduction ends. The piece of crust in between the craton and the spreading ridge, to the right of the craton, is not subducted and retains its crustal thickness (Figure 23b). On the opposite side of the craton, there is also a section of crust that is not subducted. When the craton moves towards the subduction zone, the subduction stops as soon as they make contact. This prevents a part of the crustal material from the other side from subducting, leaving the section of crust on the left side of the craton intact (Figure 23b).

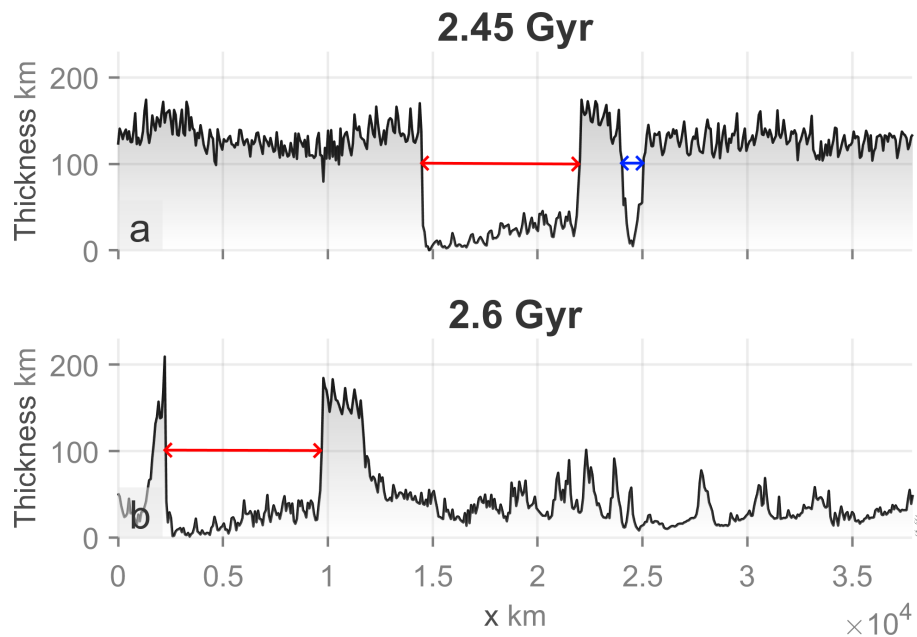


Figure 23: Crustal thickness at 2.45 Gyr and 2.60 Gyr for the case with one craton and 150 MPa yield stress. The red arrows signify the craton, blue arrow signifies the spreading centre.

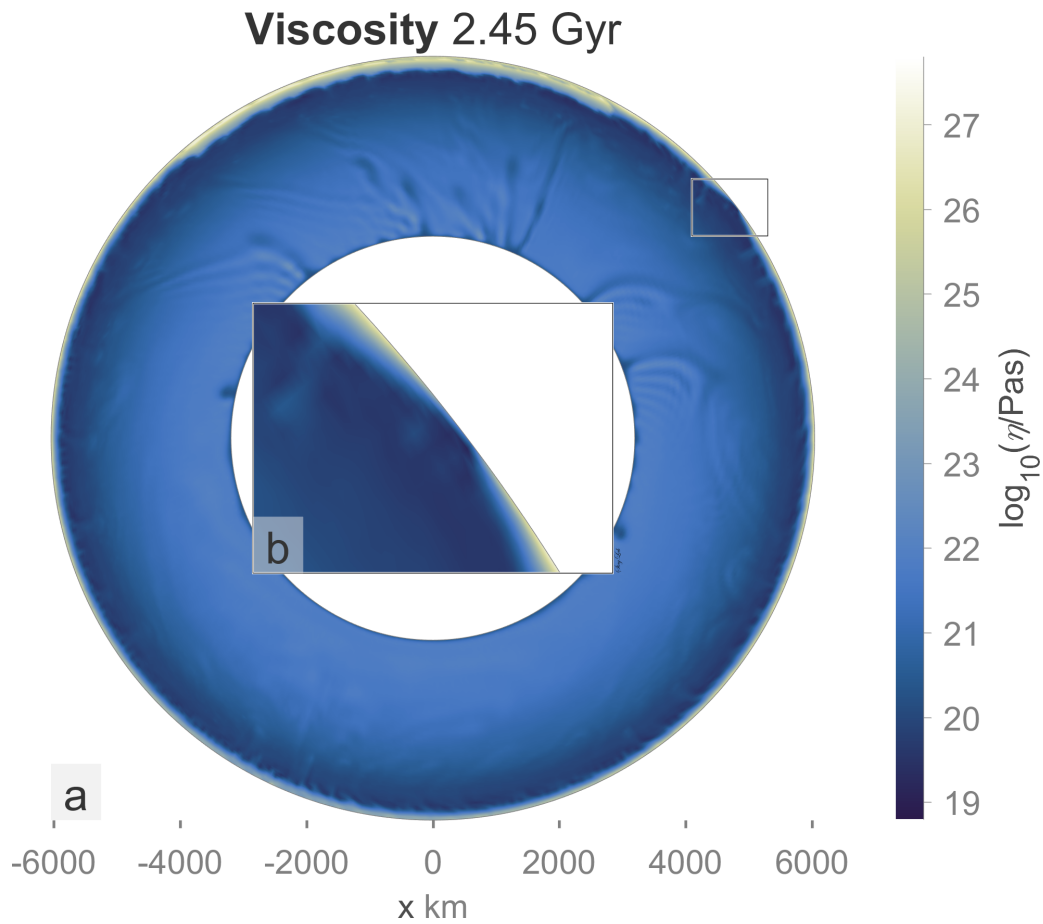


Figure 24: The spreading ridge, close to the craton.

The total mean crustal thickness decreases with the addition of cratons, because the cratons have significantly lower added crustal thickness than the remaining crust. This reduces the total average artificially. Because of this effect, the cratonic areas were excluded for the calculation of the mean crustal thickness. As a result, one can now observe that the crustal thickness increases first and stabilises at a certain time. It seems to reach an equilibrium after 2 - 3 Gyr in the infinite yield stress cases. The zero, one and two craton cases end up with approximately the same crustal thickness, the three and four craton cases have a slightly thicker crusts (Figure 25).

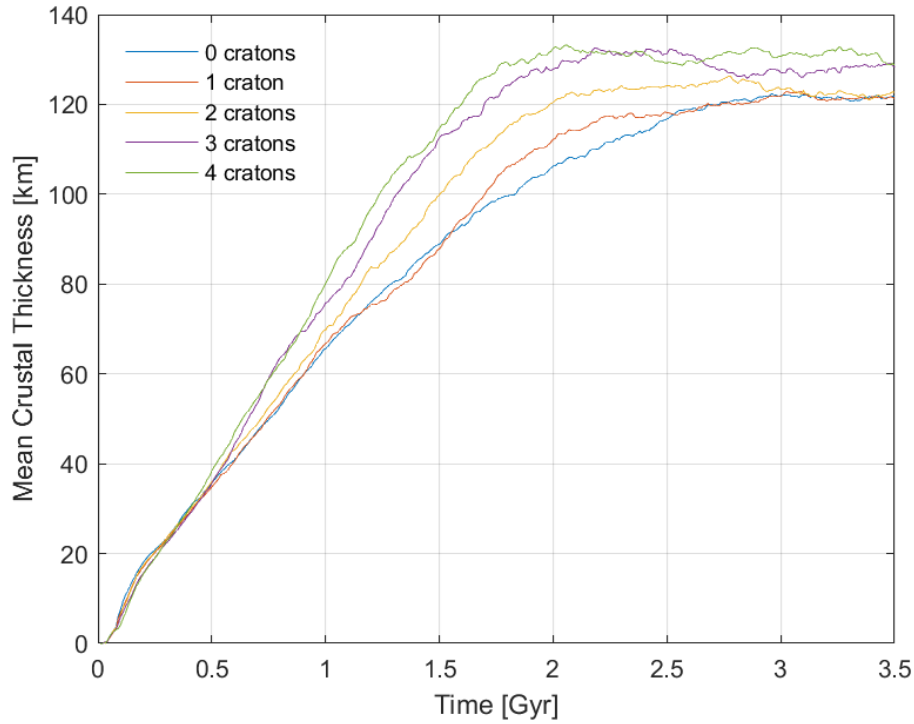
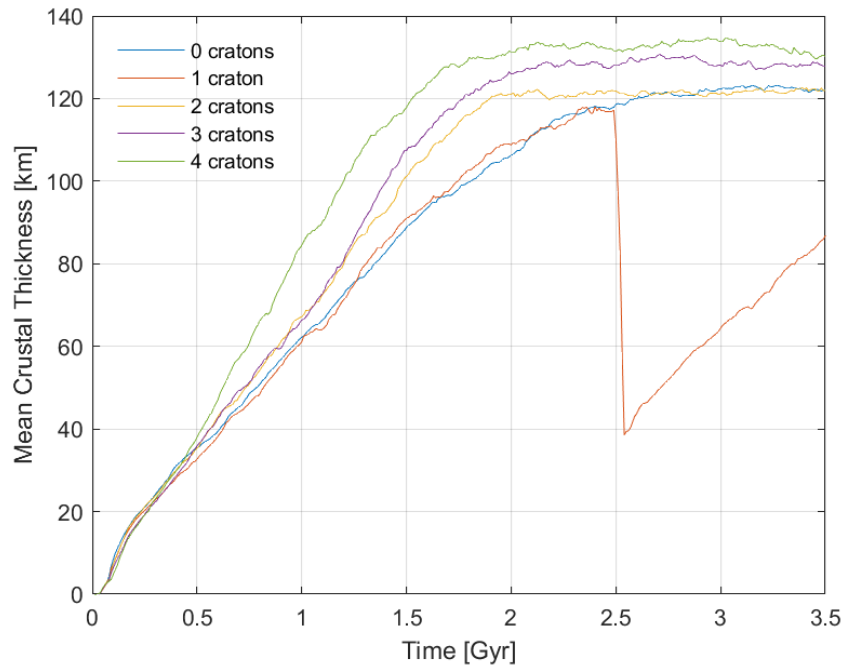
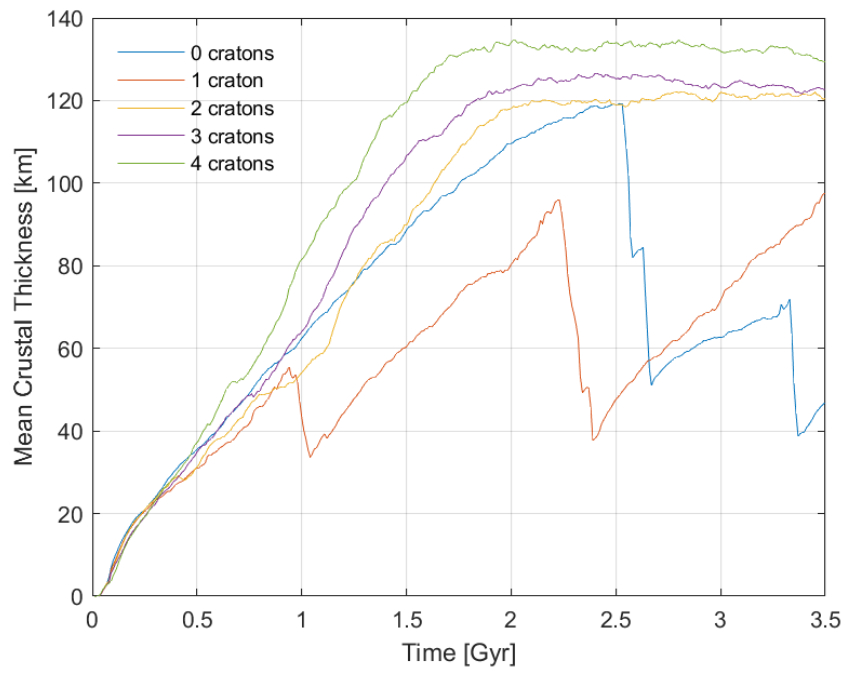


Figure 25: Mean crustal thickness excluding cratons, in models with different number of cratons and infinite yield stress

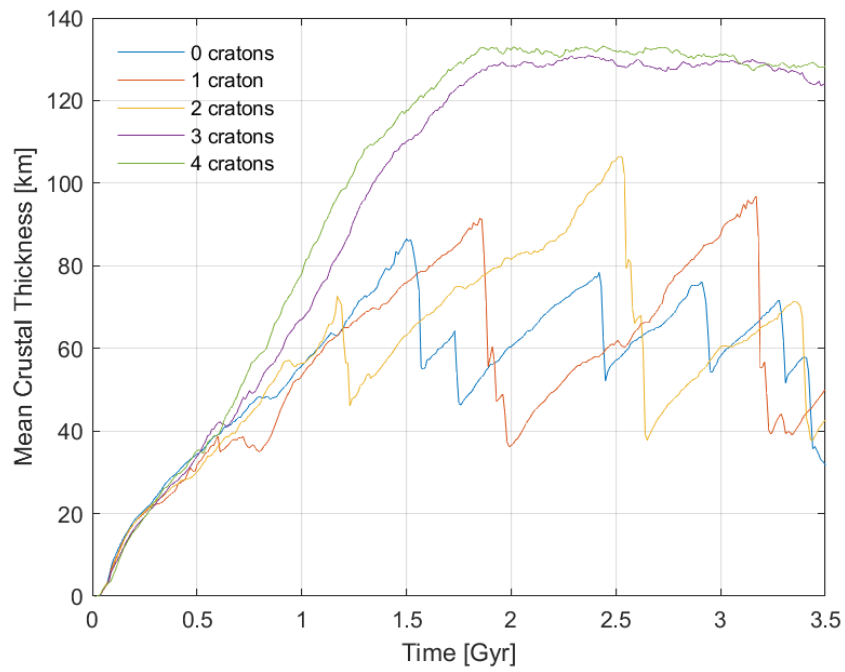
For the other cases with lower yield stresses, the crustal thicknesses depends highly the timing of overturns. Figure 26 shows comparisons of crustal thicknesses for cases with different number of cratons and yield stresses of 40 - 150 MPa. The cases with more overturns yields lower crustal thicknesses than the ones with fewer overturns. However, the crustal thickness may decrease to between 40 and 60 km after just one single overturn, which is only 1/3 of the crustal thickness for cases without overturns. New crust is produced through eruptions, while the overturn is still in progress, preventing the crustal thickness decreasing further. The cases that do not experience any overturns end up with approximately the same crustal thickness, regardless of the number of cratons.



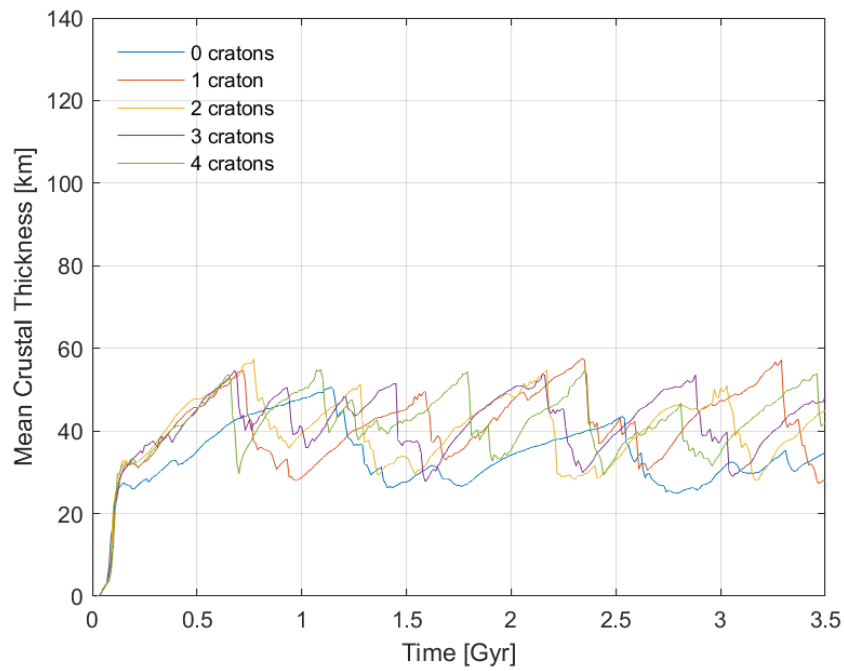
(a) 150 MPa



(b) 100 MPa



(c) 80 MPa



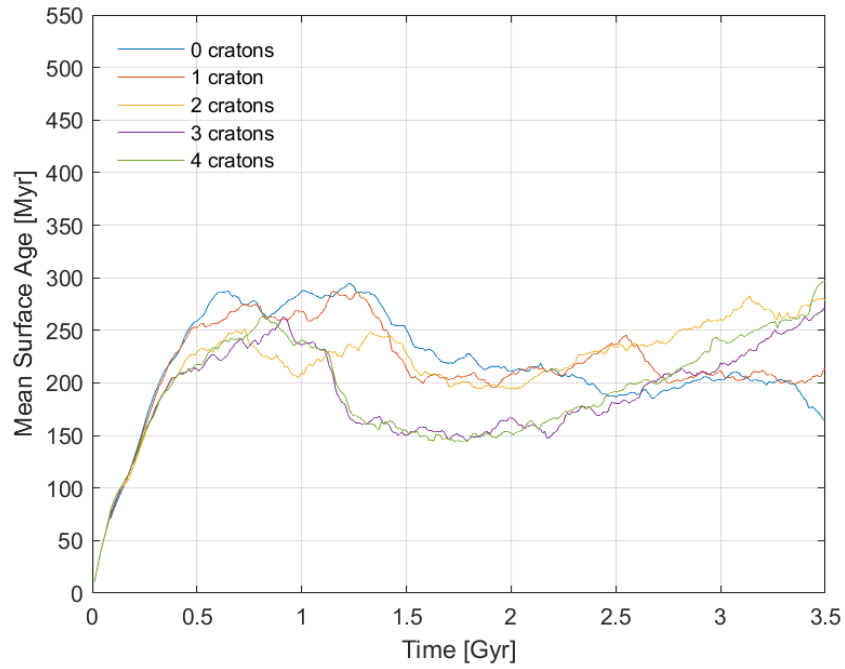
(d) 40 MPa

Figure 26: Crustal thickness for areas without cratons.

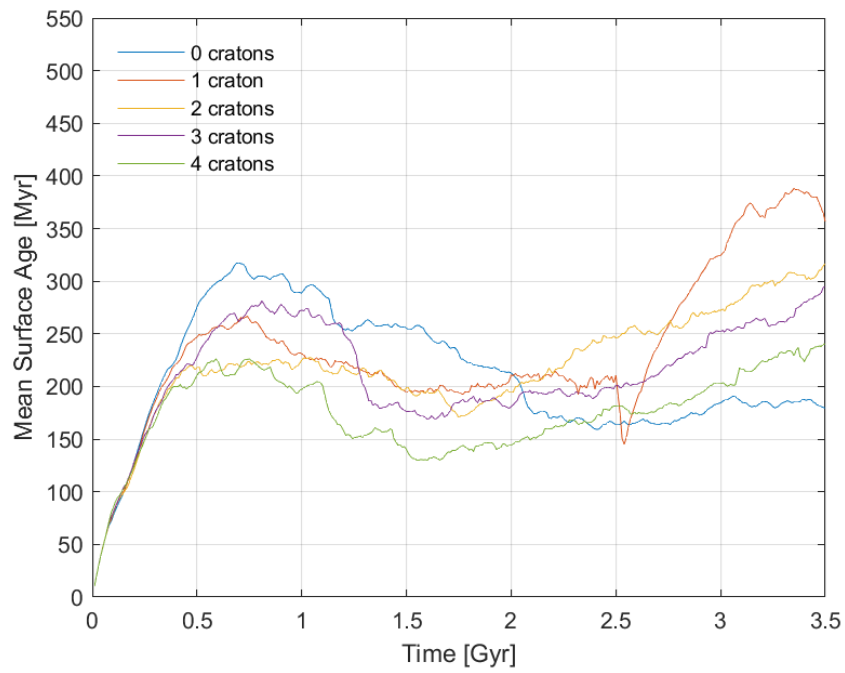
3.6 Surface age

In this model setup, the surface is renewed in two ways: first through global overturn events and second through eruptions onto the surface. Surface eruptions are less frequent on the cratons, and more important on the remainder of the surface. Therefore, the cratons have been excluded when calculating the mean surface age. The surface ages for the cases that do not experience overturn events is generally < 350 Ma (Figure 27). It reaches a maximum of 200 - 350 Myr after 0.5 - 1.5 Gyr and then it decreases to 100 - 200 Myr, where it either stays stable or increases again.

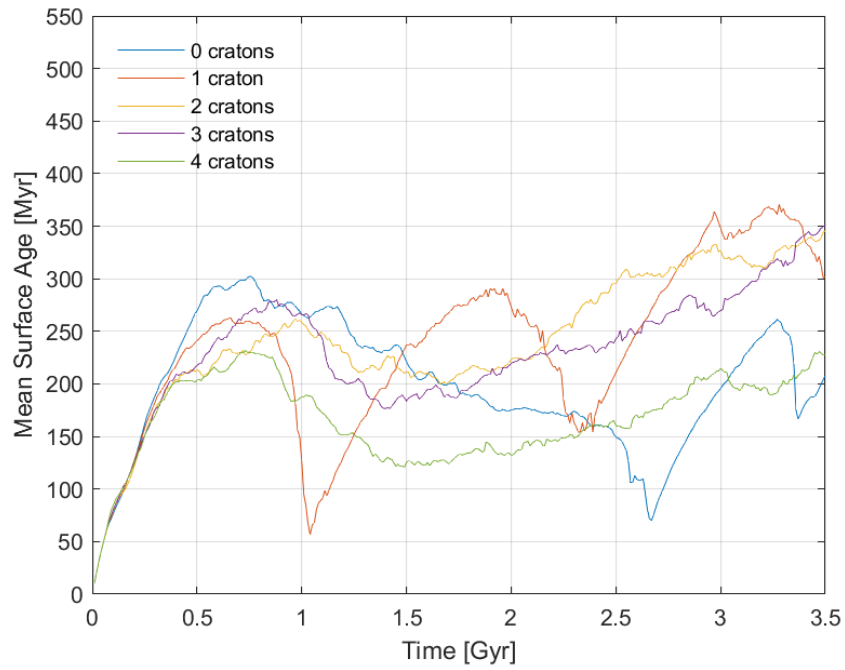
The sharp dips in the mean surface age correlates with the subduction periods. The surface age drastically decreases when subduction is initiated. For the cases with 40 MPa, most visible in the case without cratons, the surface age increases further than the other cases after subduction stopped (Figure 27e). For the cases with higher yield stresses, the mean surface age lies between 300 and 400 Ma, whereas for the case with 40 MPa yield stress, the mean age reaches > 500 Ma, after the subduction period is terminated. The same tendency of higher ages succeeding overturn events is shown for some of the other cases with, although it is less apparent.



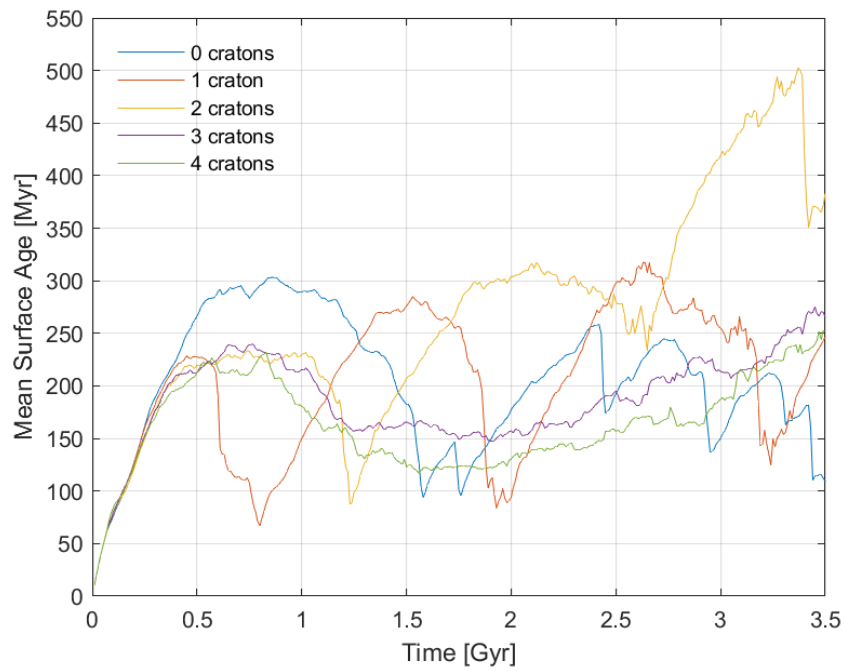
(a) Infinite yield stress



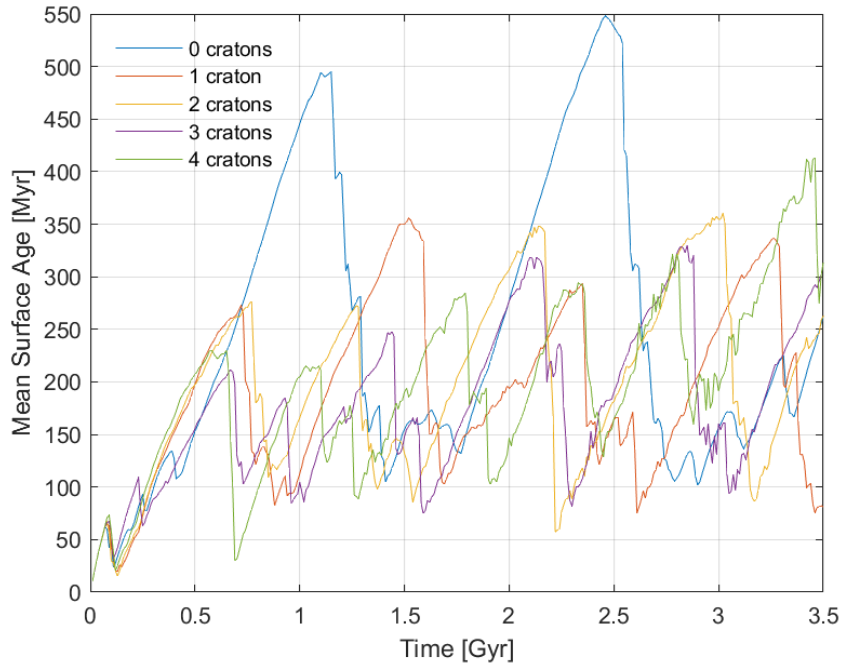
(b) 150 MPa



(c) 100 MPa



(d) 80 MPa



(e) 40 MPa

Figure 27: Surface age for areas without cratons on models with varying number of cratons.

The surface distribution plot shows the fraction of the surface that is of a certain age after 1 Gyr (Figure 28). For the case without cratons there is a very small amount of the surface that has an age of 1 Gyr, meaning that they have not been recycled. The age distributions for the cases with lower yield stresses depend mostly on when in the evolution the plot is made. The surface distribution changes fast with the subduction events. So when the peak is at or close to 0 Gyr, the model has just experienced an overturn. The peak at 1 Gyr signifying the craton, which will age with the model.

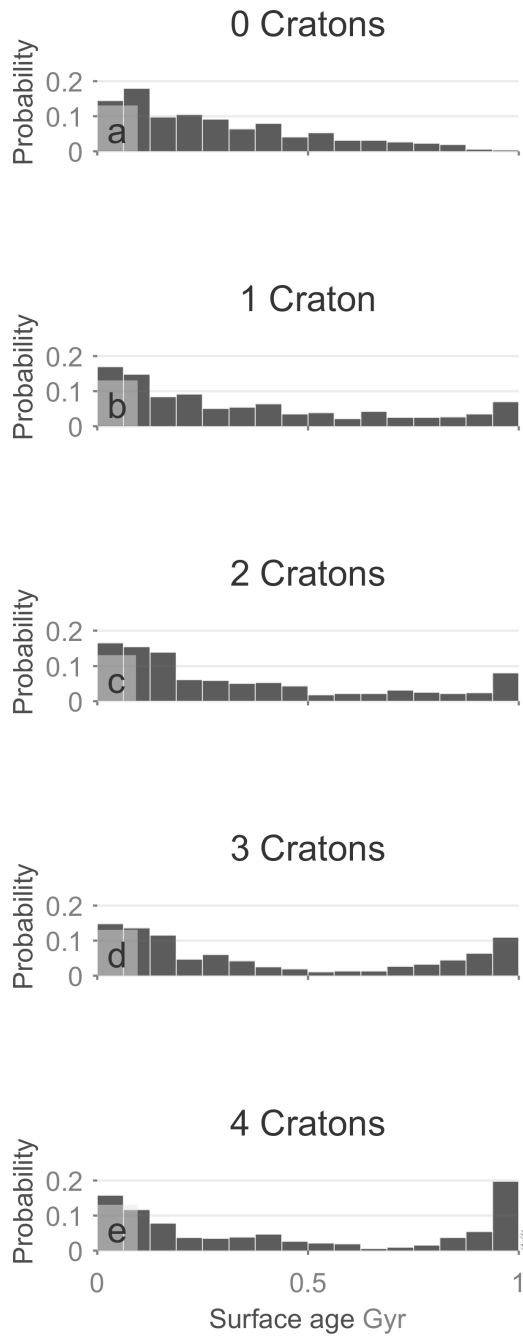


Figure 28: Surface distribution at 1 Gyr

The surface age distribution for the case with one craton and 100 MPa yield stress, before, during and after an overturn period is shown in Figure 29. The overturn period lasts from 0.97 to 1.05 Gyr. Before the subduction starts, the surface age is distributed

almost equally up to 0.75 Gyr. When the overturn starts the surface age distribution peaks at 0 Gyr, because of the renewed surface. After the overturn and subduction is no longer present, the peak moves to higher ages. The viscosity field plots for the same time steps as the surface age distribution, shows the craton moving and the surface being subducted (Figure 30).

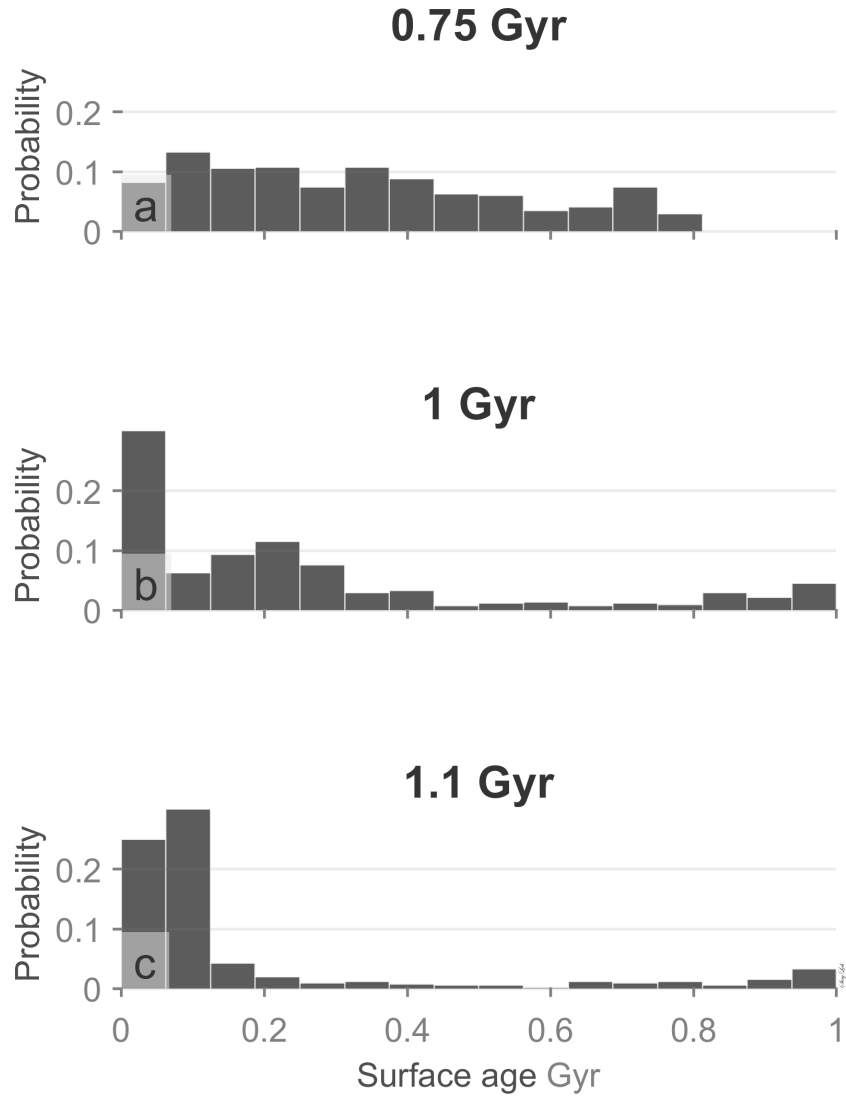


Figure 29: Surface distribution before, during and after overturn, for the case with one craton and 100 MPa yield stress.

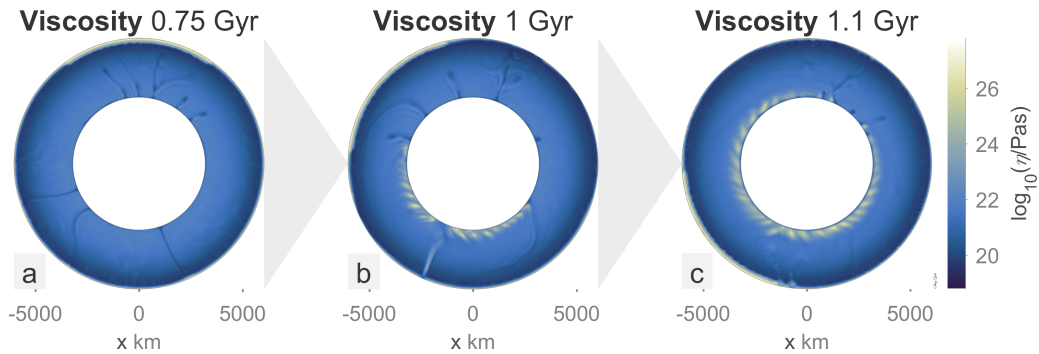


Figure 30: Viscosity of the evolution in the same case as figure 29.

3.7 3D models

Four 3D cases with one pre-imposed craton were modelled using yield stresses of practically infinite (1×10^6 MPa), 150 MPa, 100 MPa and 80 MPa, to compare with the 2D models. The cases were run for ~ 2.0 Gyr rather than 3.5 Gyr, due to computing time constraints. Whereas the 2D models with one craton experienced overturn at 150 MPa and less, the corresponding 3D case experienced overturn event in the cases with, 100 MPa and 80 MPa yield stress. For the 2D case with 100 MPa, overturn was initiated at ~ 1 Gyr, while the corresponding 3D case initiated overturn at ~ 1.5 Gyr. For the 80 MPa cases the overturns were initiated at ~ 0.8 Gyr and ~ 0.9 Gyr for the 2D and 3D respectively. The 3D case with 150 MPa yield stress was not computed for as long a time as the 2D case, so the overturn may still be initiated in this case. The difference in time of overturn initiation is rather short, suggesting that the two model geometries follow a similar evolution.

Figures 31 and 32 shows an overturn event in the 3D model with 80 MPa yield stress. The craton mainly has a "continental" composition, the parts of "crust" on the craton area is caused by eruptions on the surface. The overturn event is initiated by a spreading adjacent to the craton, (Figure 31), major eruption of mantle material is initiated and spreads as the overturn progresses. The craton moves south and ends up at the south pole. There is still a region of "crustal" material that is preserved at the edge of the craton while it moves, this may have the same explanation as for the 2D model, compare to Section 3.5; Figure 23. Since the spreading centre is dipping away from the craton, the crustal material in between the craton and the spreading is preserved.

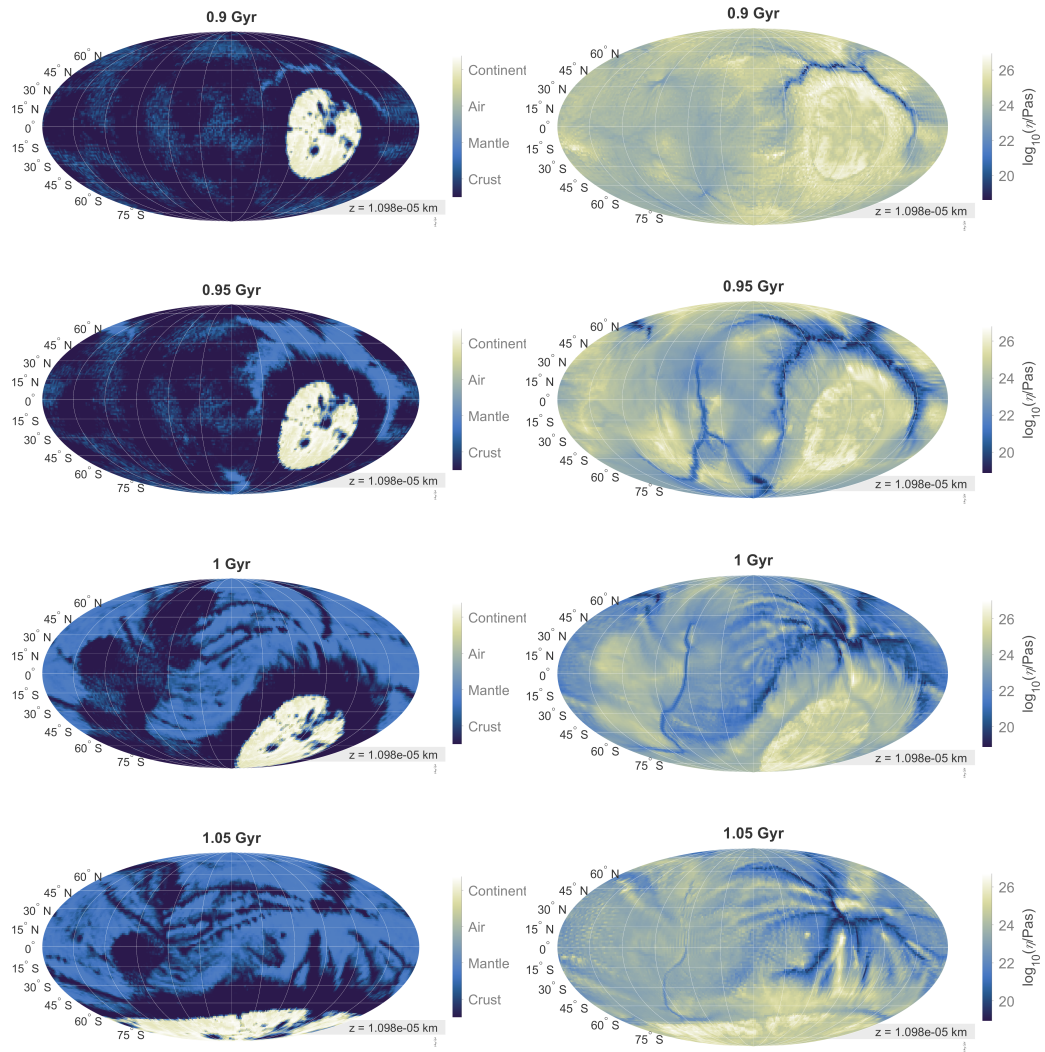


Figure 31: Evolution of an overturn event in the 3D model with one craton and 80 MPa yield stress, shown by composition and viscosity fields. Spreading is initiated above the craton.

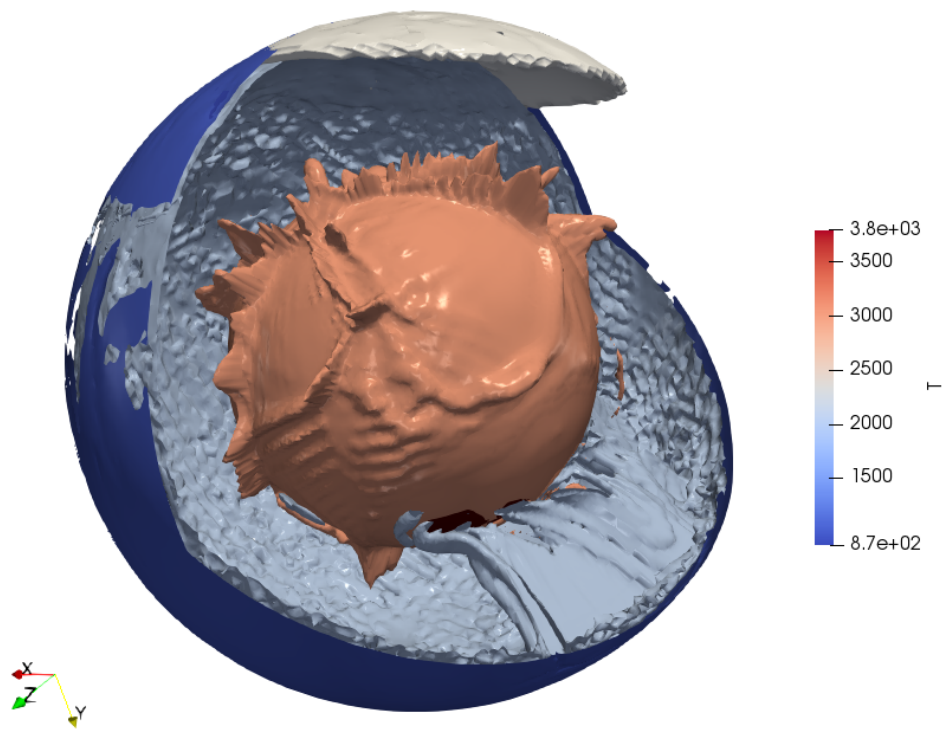


Figure 32: Subducting slab during the overturn event in Figure 31.

4 Discussion

This study focuses on the impact of cratons on the mantle dynamics and proposed overturn events on Venus, studied by varying yield stress and number of cratons, in thirty 2D models and additional 3D models. The number of pre-imposed cratons are found to have an impact on mantle movement and the initiation of overturn events. Aspects of the mantle that was examined to understand the connection between mantle and cratons were: plumes and slabs in the mantle, thermal evolution, crustal thickness and surface age.

4.1 Stagnant and episodic lid

To understand the connection between pre-imposed cratons and the initiation of overturn events, two methods are used to indicate the overturns. These are the number of slabs per time and the surface mobility (Figures 9 and 7). The surface mobility indicates overturns as periods via surface motion, the number of slabs diagnostic indicates overturns as periods but also provide a measure for the number of subduction zones. This extra information can indicate the spacial impact each slab has on the surface. Both diagnostics show that the initiation of overturns is affected by the yield stress and the number of cratons on the surface. There are several reasons for the variation in the timing of overturn initiation. The main reason is the yield stress, subduction is favoured with lower yield stresses. However, the cratons may also play a role by affecting the mantle dynamics in different ways.

Cratons are heterogeneities on the upper boundary of the mantle, because of their rheology and thereby the viscosity (Figure 5). These heterogeneities can focus stress at the craton margins and facilitate breaking of the lithosphere, causing subduction (Rolf and Tackley, 2011). Cratons feature a lower surface heat flow than non-cratonic areas and therefore produce a thermal blanketing effect, which can decrease the total heat loss from the interior. However, this effect does not necessarily cause a warmer mantle and lower heat loss. The partial insulation caused by cratons may decrease the viscosity and thereby increase the velocities in the mantle. This will again speed up subduction, causing more frequent overturn episodes. This also increases heat loss from the mantle, cooling it down. The effect is greatest for large cratons and decreases with decreasing craton

size (Lenardic et al., 2005). However, the thermal insulation may not be very strong for any of these cases, since this increase in temperature could increase the melt production underneath the craton and cause more vigorous eruptions on the cratons. This is not the case and the excess heat is not trapped underneath the cratons, but escape from other parts of the surface, like the spreading ridges that sometimes are formed near the cratons.

Melting and crustal production may change the timing of overturns. All eruption in the models happens directly on the surface, increasing the thickness of the crust. The crust is buoyant as long as it is thin, but if it grows thick enough to cross the phase transition from basalt to eclogite, at 65 km depth, the density increases and the crust becomes heavier and thereby may break and initiate overturn (Lourenço et al., 2016).

The reason for the pattern of overturn initiation shown by Figure 9 can be related to all of these effects. The case with one craton may have the largest effect on the mantle in the form of a heterogeneity and thermal blanketing. In the case with two cratons the effects are a little less pronounced, because it has a smaller impact on the mantle. However, there must be an explanation for why the cases with three and four cratons yields subduction at lower yield stresses than the case without cratons. This may have a connection to the convection cell pattern produced by the varying number of cratons on the surface (Figure 20). The cases with multiple cratons decreases the size of convection cells in the mantle, this decrease may cause a more equal distribution of stresses in the mantle, whereas fewer convection cells may help focus the stress in one area and thereby facilitate overturns. More in depth study on how convection cells relate to cratons is needed in order to examine this correlation.

The cases with one craton initiates overturn already at 150 MPa yield stress, while the cases with no cratons initiates overturn at 100 MPa yield stress, showing that the one craton may help enable overturn events. However the real difference in yield stress needed to produce overturns for cases with zero and one craton is not known. If this difference is small, there is a possibility that the initiation of the overturn at 150 MPa is a coincidence and that one craton has a limited effect on the overturn initiation. An observation that supports the proposal that the one craton has an impact is that the overturns in the 80

and 100 MPa cases are initiated at an earlier time compared to the zero craton equivalent cases. More systematic studies with yield stresses in between 100 MPa and 150 MPa must be examined to understand the real difference in yield stress needed to produce overturns with zero and one craton.

The cases with 20 MPa yield stress show a convection regime which is close to mobile lid and is therefore less interesting for Venus. There are also several of these models where the cratons are subducted at an early stage in the simulation. This is not favourable when the object of the thesis is to examine the effect of cratons on the mantle dynamics. These models are therefore only partly considered.

4.2 Mode of overturns

The cratons impact the mantle dynamics by changing the convection cell and plume patterns. The overturns in models with cratons are usually initiated on the opposite hemisphere to the craton, or as far as possible away from them. This may be related to the upwellings at the underside of the cratons, causing downwelling areas at the opposite hemisphere. The upwelling can produce rifting and spreading close to the craton (Figure 24). The overturn is then initiated by the downwelling produced on the opposite side from the spreading.

When cratons collide in the models, they tend to stick together and seems not to separate again. This is generally not the case for Venus or Earth. On Venus, the tesserae regions are not clustered together in one spot, but spread in four distinct areas (Figure 3). On Earth, the continents collide and break up again in cycles (Buitert and Torsvik, 2014). One of the reasons for the break ups of continents may be plumes (Storey, 1995), although it is still debated whether plumes are in fact strong enough to break up continents unaided. When continents collide on Earth, there are weak sutures formed at the location of the collisions. In the modelled craton collisions, these weak zones are not implemented, which makes break up, by plumes or other mechanisms, more difficult. Authors have improved mantle models with cratons by adding weak zones at the edges when modelling continents on Earth (Rolf and Tackley, 2011; Yoshida, 2010; Lenardic et al., 2003). This addition somewhat improves the cratons ability to break apart. Break up of cratons may also be

easier in 3D models than in 2D, because of the ability of the plates to move relative to each other in all directions, rather than just two directions like in the 2D models.

4.3 Thermal evolution

The mean mantle temperature increases with time for all cases, except those with frequent overturn events (40 and 20 MPa). This is probably caused by the models initial conditions. The temperature of an actual planet would begin hot and cool down through time. The effective cooling is caused by the loss of radiogenic heating capability. Since the radiogenic material decays over time, the heat production will diminish. In the model, on the other hand, the initial heating is constant and equilibrium will be reached instead of the decrease in temperature (Figure 15). The equilibrium is reached for all stagnant lid cases except for the case with one craton and infinite yield stress (Figure 15e), meaning that in this model, the internal heating may still dominate over heat loss from the surface.

The drastic drops in temperature can be correlated with the initiation of the overturn events. The cool slabs descend all the way down to the CMB where they slowly mix with the rest of the mantle. The figures showing the evolution of overturn events, show the surface subducting down to the CMB (Figures 10, 11, 13 and 14). The material at the CMB generally stays there for a long time, before getting remixed into the mantle. This inhibits the production of plumes, slowing down the heat loss by volcanism. However, this seems to be insignificant compared to the cooling effect of the slabs, so that the cases with frequent overturns show a significantly lower mean mantle temperature than the stagnant lid cases.

4.4 Plumes

The number of cratons is essential to the number of plumes and convection cells present in the mantle. The lowest number of mid-mantle plumes is found in the cases with one craton and thereafter the number of plumes increase with the addition of more cratons. The highest number of detected plumes is in the case with no cratons (Figure 18). The overturn events in the models causes movement in the mantle and disturbance of the plumes, making them hard to detect. This is shown by a distinct lack of mid-mantle plumes in the periods where subduction is active, and some time after (Figure 18). The

disappearance of plumes may be due to horizontal movement in the mantle, making it hard for StagLab to recognise them.

The number of convection cells in the mantle is influenced by several parameters, among them internal heating and the viscosity profile in the mantle (Crowley and O’Connell, 2012), however, another important factor is the number of cratons. In Figure 21 d, e and f the model with one craton shows degree-1 convection, the material in the lower mantle is moving towards the underside of the craton. From there it is moving up towards the craton and out in the upper mantle on each side of the craton. This fits with the assumption that large cratons favour larger convection cells (Phillips and Coltice, 2010). The case with no cratons favours a higher number of convection cells that decreases through time (Figure 21 a, b and c). This can be seen by the horizontal velocity plots, these show the material in the case with one craton (figure 21e) moving towards the underside of the craton, whereas in the case without cratons (figure 21b) the movement is more clearly divided into cells. The radial velocity in the plumes for the zero craton case is also much higher than for the one craton case (Figure 21c and f), because it is supported by the horizontal movement and not disturbed by it. In the one craton case the horizontal movement is stronger than the vertical movement inside the plume.

4.5 Crustal thickness and surface age

The crust on the non-cratonic surface is produced by melting and eruptions. There is also crust on the cratons, this is however, pre-imposed cratonic crust and is not taken into consideration with the non-cratonic crust. The difference in newly added crustal thickness between the cratonic and the non-cratonic areas is due to smaller amounts of eruptions on the cratons (Figure 25). The cratons are relatively thick compared to the remainder of the surface. Therefore the thermal boundary layer is also thicker and it is more difficult for the mantle temperatures to exceed the solidus. This causes less melting and therefore less eruptions, and thinner added crust.

The presence of a craton may also help preserve parts of the non-cratonic surface through an overturn event. The crustal thickness before and after an overturn are presented in Figure 23. In Figure 23b, non-cratonic material is preserved at both edges of the craton.

One of the preserved parts are caused by the spreading centre not being at the craton margin, but slightly removed from it, while the other part is due to the craton ending the subduction by coming in contact with the downwelling before all surface material was subducted.

The surface for all the models is renewed even when overturns are not occurring. This is evident from that the surface age increases to a certain point and then decreases and reaches a steady state (Figure 27). When the temperature is low there is little melting and eruption, and a slow renewal of the surface. When the mantle heats up the eruptions became more efficient and the surface age decreases somewhat. The distribution of surface ages after 1 Gyr for cases with different number of cratons also show that the surface is renewed (Figure 28). The peak at 1 Gyr for the models with cratons are the cratons themselves. Most of the remaining surface has a much younger age, consistent with renewal of the surface through eruption. The parts of the surface that still retain an old age, but are not part of the cratons, can be a result of the initiation of rifting close to, but not right at the edge of the cratons, preserving a piece of non-cratonic crust on the surface.

A drastic decrease in surface age signifies the overturn episodes, where the surface is renewed rapidly by subduction. In most of the cases where overturns are occurring, the surface reaches higher ages than the stagnant lid models. This might be related to the disturbance of the upwelling areas during an overturn, and the cooling of the mantle by the subduction of large parts of the surface. The cool slabs subduct down to the core mantle boundary and stay there a time before getting remixed into the mantle, this blocks the plumes and decreases the eruption activity, causing higher surface ages. The surface age increases until a new overturn is initiated, the oldest ages are found right before initiation of a new overturn.

There is a possibility of an overestimation of surface ages for all the models. In reality, large portions of the magmatic material in a planet should be intrusive, and would therefore not impact the surface age. However, since a molten upper mantle is assumed, the partial melting causes erupted material to automatically be emplaced on the surface, meaning that there is no intrusive magmatism and all the melt that is produced is

extrusive, this may cause some underestimation of surface age.

4.6 3D models

Four 3D models with one pre-imposed craton of 10 % coverage and yield stresses of practically infinite (1×10^{12} MPa), 150 MPa, 100 MPa and 80 MPa were computed. They were computed for a shorter time than the 2D models, however, both the case with 100 MPa and 80 MPa yield stress yielded overturn. The difference in timing between the initiation of overturn in the 2D and 3D cases was also quite short, 0.5 Gyr for the 80 MPa cases and 0.1 Gyr for the 100 MPa cases. The geometry of the models may have an impact on the initiation of overturns, where initiation is easier to achieve in 2D cases than in 3D cases (Rolf et al., 2018), however, the short offset in time showed here, points to a similar evolution.

4.7 Comparison to Venus

The model of Venus created with the StagYY code is greatly simplified. The cratons are modelled as Earth's Archean cratons with similar composition and thickness. This does probably not apply for the tesserae on Venus, since both the thickness and the composition is unknown. From morphology and radiance, the composition could be more felsic, however, other explanations such as grain size and weathering may also account for the differences in radiance (Gilmore et al., 2015). There is great uncertainty on whether the tesserae regions on Venus are in fact comparable to Earth's continents. The tesserae regions are also scattered about the surface, several of them are more or less situated in clusters, but these are separated by volcanic plains and other structures (Ivanov and Head, 2011). In all models with episodic lid and cratons, the cratons collide and do not part again. The most likely reason for this is the model itself, and introducing weak zones at the edges of the cratons may improve this.

The crustal thickness varies drastically from episodic to stagnant lid. The episodic lid models produced here, yielded crustal thicknesses of 30 - 80 km, depending on the frequency of overturns. The cases with most frequent overturns and crustal thicknesses of 30 - 40 km gives the best fit with previously estimated mean crustal thicknesses for Venus of 20 km (Phillips and Hansen, 1994) and 8-25 km (James et al., 2013). The stagnant lid

models with crustal thicknesses of 120 - 130 km, does not fit with the previous estimates, suggesting that the episodic lid model is more accurate in this regard.

The surface ages for the stagnant lid model lie between 200 and 300 Myr, while the episodic lid models vary greatly depending on the frequency of overturns and yield values between 100 and 500 Myr. The surface age of Venus is estimated by (Strom et al., 1994; Schaber et al., 1992) to be ~ 500 Myr. There are only two cases that reaches this age: the case with zero cratons and 40 MPa yield stress reaches this age after 1 Gyr and 2.5 Gyr, while the case with two cratons and 80 MPa yield stress reaches this age after 3.25 Gyr (Figure 27). The surface age of the episodic models depend highly on the timing and frequency of overturns, but these models are able to produce surface ages of 500 Myr. As discussed in chapter 4.5 this may be due to underestimation of surface ages made by the mode of eruption implemented in the model.

5 Conclusions

The effect of pre-imposed cratons on the mantle dynamics has been examined by studying model cases with varying yield stresses and number of cratons. By looking into aspects of the mantle dynamics: slabs and plumes, thermal evolution, crustal thickness and surface age, the findings can be summarised in three points:

- The number and timing of overturns is partly influenced by pre-imposed cratons. Imposing cratons on the surface of the models changes the flow pattern in the mantle and thereby the initiation of overturns. For a higher number of cratons (three and four), overturns are prevented. This may be due to the impact cratons have on the wavelength of convection in the mantle, spreading the stress, rather than concentrating it in a single area. It is still unclear whether one imposed craton promotes initiation of overturn or whether it has a limited effect.
- The cratons may help preserve non-cratonic material through global overturn events. When overturns are initiated, the cratons are moved towards the downwelling area. When they come into contact, the subduction ceases, this may happen before the global resurfacing is finished, leaving certain parts of the non-cratonic crust intact.
- The calculated crustal thickness differs for stagnant and episodic lid cases. The best fit with assumed values for Venus are the episodic lid cases with crustal thicknesses of 30 - 80 km. The assumed surface ages from crater statistics of ~ 500 Myr are produced in some of the cases featuring an episodic lid convection. However, the underestimation of surface ages, caused by the volcanism always being extrusive, may be one reason for the difficulty of producing higher surface ages to better match estimates.

Further work is needed to further the understanding of the cratons impact on the mantle. More work on the connection between convection cells and cratons is needed to understand the connection between cratons and global overturns. A more thorough examination of cases with zero and one craton and yield stresses in between 100 MPa and 150 MPa may show whether the single imposed craton really promotes overturn initiation. More 3D cases are needed to understand the difference in overturn initiation time for 2D and 3D models. Lastly, further exploration of Venus is needed to gather necessary data for producing better, more realistic numerical models of Venus' mantle.

References

- Anderson, F. S. and Smrekar, S. E. (2006). Global mapping of crustal and lithospheric thickness on venus. *Journal of Geophysical Research: Planets*, 111(E8).
- Armann, M. and Tackley, P. J. (2012). Simulating the thermochemical magmatic and tectonic evolution of venus’s mantle and lithosphere: Two-dimensional models. *Journal of Geophysical Research: Planets*, 117(E12).
- Basilevsky, A., Ivanov, M., Head, J., Aittola, M., and Raitala, J. (2007). Landing on venus: Past and future. *Planetary and Space Science*, 55(14):2097–2112.
- Basilevsky, A. T. and Head, J. W. (2003). The surface of venus. *Reports on Progress in Physics*, 66(10):1699.
- Bercovici, D. and Ricard, Y. (2014). Plate tectonics, damage and inheritance. *Nature*, 508(7497):513.
- Bindschadler, D. (1995). Magellan: A new view of venus’ geology and geophysics. *Reviews of Geophysics*, 33(S1):459–467.
- Brown, C. D. and Grimm, R. E. (1997). Tessera deformation and the contemporaneous thermal state of the plateau highlands, venus. *Earth and planetary science letters*, 147(1-4):1–10.
- Buiter, S. J. and Torsvik, T. H. (2014). A review of wilson cycle plate margins: A role for mantle plumes in continental break-up along sutures? *Gondwana Research*, 26(2):627–653.
- Campbell, B. A. (1999). Surface formation rates and impact crater densities on venus. *Journal of Geophysical Research: Planets*, 104(E9):21951–21955.
- Campbell, I. H. and Griffiths, R. W. (2014). Did the formation of d cause the archaean–proterozoic transition? *Earth and Planetary Science Letters*, 388:1–8.
- Cheng, K. W., Rozel, A., and Tackley, P. (2018). Cratons on venus in global thermochemical convection models. In *AGU Fall Meeting Abstracts*.
- Crameri, F. (2017). Planetary tectonics: Sinking plates on venus. *Nature Geoscience*, 10(5):330.

- Crameri, F. (2018). Geodynamic diagnostics, scientific visualisation and staglab 3.0. *Geoscientific Model Development*, 11(6):2541–2562.
- Crowley, J. W. and O’Connell, R. J. (2012). An analytic model of convection in a system with layered viscosity and plates. *Geophysical Journal International*, 188(1):61–78.
- Davaille, A., Smrekar, S., and Tomlinson, S. (2017). Experimental and observational evidence for plume-induced subduction on venus. *Nature Geoscience*, 10(5):349.
- De Pater, I. and Lissauer, J. J. (2015). *Planetary sciences*. Cambridge University Press.
- Donahue, T. and Russell, C. (1997). The venus atmosphere and ionosphere and their interaction with the solar wind: An overview. In *Venus II: Geology, Geophysics, Atmosphere, and Solar Wind Environment*, page 3.
- Fowler, A. and O’Brien, B. (2003). Lithospheric failure on venus. *Proceedings of the Royal Society of London. Series A: Mathematical, Physical and Engineering Sciences*, 459(2039):2663–2704.
- Gilmore, M., Treiman, A., Helbert, J., and Smrekar, S. (2017). Venus surface composition constrained by observation and experiment. *Space Science Reviews*, 212(3-4):1511–1540.
- Gilmore, M. S., Mueller, N., and Helbert, J. (2015). Virtis emissivity of alpha regio, venus, with implications for tessera composition. *Icarus*, 254:350–361.
- Hansen, V. L. (2015). Impact origin of archean cratons. *Lithosphere*, 7(5):563–578.
- Hansen, V. L. (2018). Global tectonic evolution of venus, from exogenic to endogenic over time, and implications for early earth processes. *Philosophical Transactions of the Royal Society A: Mathematical, Physical and Engineering Sciences*, 376(2132):20170412.
- Harris, L. B. and Bédard, J. H. (2014). Crustal evolution and deformation in a non-plate-tectonic archaean earth: Comparisons with venus. In *Evolution of Archean crust and early life*, pages 215–291. Springer.
- Hernlund, J. W. and Tackley, P. J. (2008). Modeling mantle convection in the spherical annulus. *Physics of the Earth and Planetary Interiors*, 171(1-4):48–54.

- Herzberg, C. and Rudnick, R. (2012). Formation of cratonic lithosphere: An integrated thermal and petrological model. *Lithos*, 149:4–15.
- Ivanov, M. and Basilevsky, A. (1993). Density and morphology of impact craters on tessera terrain, venus. *Geophysical research letters*, 20(23):2579–2582.
- Ivanov, M. A. and Head, J. W. (2011). Global geological map of venus. *Planetary and Space Science*, 59(13):1559–1600.
- Ivanov, M. A. and Head, J. W. (2013). The history of volcanism on venus. *Planetary and Space Science*, 84:66–92.
- James, P. B., Zuber, M. T., and Phillips, R. J. (2013). Crustal thickness and support of topography on venus. *Journal of Geophysical Research: Planets*, 118(4):859–875.
- Kreslavsky, M. A., Ivanov, M. A., and Head, J. W. (2015). The resurfacing history of venus: Constraints from buffered crater densities. *Icarus*, 250:438–450.
- Lenardic, A., Moresi, L.-N., Jellinek, A., and Manga, M. (2005). Continental insulation, mantle cooling, and the surface area of oceans and continents. *Earth and Planetary Science Letters*, 234(3-4):317–333.
- Lenardic, A., Moresi, L.-N., and Mühlhaus, H. (2003). Longevity and stability of cratonic lithosphere: insights from numerical simulations of coupled mantle convection and continental tectonics. *Journal of Geophysical Research: Solid Earth*, 108(B6).
- Lourenço, D. L., Rozel, A., and Tackley, P. J. (2016). Melting-induced crustal production helps plate tectonics on earth-like planets. *Earth and Planetary Science Letters*, 439:18–28.
- Mitrovica, J. and Forte, A. (2004). A new inference of mantle viscosity based upon joint inversion of convection and glacial isostatic adjustment data. *Earth and Planetary Science Letters*, 225(1-2):177–189.
- Moresi, L. and Solomatov, V. (1998). Mantle convection with a brittle lithosphere: thoughts on the global tectonic styles of the earth and venus. *Geophysical Journal International*, 133(3):669–682.

- Nimmo, F. and McKenzie, D. (1998). Volcanism and tectonics on venus. *Annual Review of Earth and Planetary Sciences*, 26(1):23–51.
- Orth, C. and Solomatov, V. (2012). Constraints on the venusian crustal thickness variations in the isostatic stagnant lid approximation. *Geochemistry, Geophysics, Geosystems*, 13(11).
- Phillips, B. R. and Coltice, N. (2010). Temperature beneath continents as a function of continental cover and convective wavelength. *Journal of Geophysical Research: Solid Earth*, 115(B4).
- Phillips, R. J. and Hansen, V. L. (1994). Tectonic and magmatic evolution of venus. *Annual Review of Earth and Planetary Sciences*, 22(1):597–656.
- Rolf, T., Coltice, N., and Tackley, P. (2012). Linking continental drift, plate tectonics and the thermal state of the earth’s mantle. *Earth and Planetary Science Letters*, 351:134–146.
- Rolf, T., Steinberger, B., Sruthi, U., and Werner, S. C. (2018). Inferences on the mantle viscosity structure and the post-overturn evolutionary state of venus. *Icarus*, 313:107–123.
- Rolf, T. and Tackley, P. (2011). Focussing of stress by continents in 3d spherical mantle convection with self-consistent plate tectonics. *Geophysical Research Letters*, 38(18).
- Romeo, I. and Turcotte, D. (2008). Pulsating continents on venus: An explanation for crustal plateaus and tessera terrains. *Earth and Planetary Science Letters*, 276(1-2):85–97.
- Romeo, I. and Turcotte, D. (2010). Resurfacing on venus. *Planetary and Space Science*, 58(10):1374–1380.
- Schaber, G., Strom, R., Moore, H., Soderblom, L. A., Kirk, R. L., Chadwick, D., Dawson, D., Gaddis, L., Boyce, J., and Russell, J. (1992). Geology and distribution of impact craters on venus: What are they telling us? *Journal of Geophysical Research: Planets*, 97(E8):13257–13301.

- Smrekar, S. E., Stofan, E. R., Mueller, N., Treiman, A., Elkins-Tanton, L., Helbert, J., Piccioni, G., and Drossart, P. (2010). Recent hotspot volcanism on venus from virtis emissivity data. *Science*, 328(5978):605–608.
- Storey, B. C. (1995). The role of mantle plumes in continental breakup: case histories from gondwanaland. *Nature*, 377(6547):301.
- Strom, R. G., Schaber, G. G., and Dawson, D. D. (1994). The global resurfacing of venus. *Journal of Geophysical Research: Planets*, 99(E5):10899–10926.
- Svedhem, H., Titov, D., McCoy, D., Lebreton, J.-P., Barabash, S., Bertaux, J.-L., Drossart, P., Formisano, V., Häusler, B., Korablev, O., et al. (2007). Venus express—the first european mission to venus. *Planetary and Space Science*, 55(12):1636–1652.
- Tackley, P. J. (2008). Modelling compressible mantle convection with large viscosity contrasts in a three-dimensional spherical shell using the yin-yang grid. *Physics of the Earth and Planetary Interiors*, 171(1-4):7–18.
- Turcotte, D. L. (1989). A heat pipe mechanism for volcanism and tectonics on venus. *Journal of Geophysical Research: Solid Earth*, 94(B3):2779–2785.
- Turcotte, D. L. (1995). How does venus lose heat? *Journal of Geophysical Research: Planets*, 100(E8):16931–16940.
- Van Heck, H. and Tackley, P. (2008). Planforms of self-consistently generated plates in 3d spherical geometry. *Geophysical Research Letters*, 35(19).
- Weller, M., Lenardic, A., and O’Neill, C. (2015). The effects of internal heating and large scale climate variations on tectonic bi-stability in terrestrial planets. *Earth and Planetary Science Letters*, 420:85–94.
- Yoshida, M. (2010). Temporal evolution of the stress state in a supercontinent during mantle reorganization. *Geophysical Journal International*, 180(1):1–22.